Ore Geology Reviews 139 (2021) 104593

Contents lists available at ScienceDirect

Ore Geology Reviews

journal homepage: www.elsevier.com/locate/oregeorev

Sources of metals and fluids for the Taijiying gold deposit on the northern margin of the North China Craton

Jian-Guo Yuan [a,b], Hua-Feng Zhang [b], Ying Tong [a,*], Jian-Feng Gao [c,*], Rong-Ge Xiao [b]

[a] Institute of Geology, Chinese Academy of Geological Sciences, Beijing 100037, China
[b] School of Earth Sciences and Resources, China University of Geosciences, 29# Xue-Yuan Road, Haidian District, Beijing, 100083, China
[c] State Key Laboratory of Ore Deposit Geochemistry, Institute of Geochemistry, Chinese Academy of Sciences, Guiyang 550081, China

ARTICLE INFO

Keywords:
Fluid inclusions
H-O-S-Pb-Os isotopes
Magmatic hydrothermal gold deposit
Taijiying gold deposit
North China Craton

ABSTRACT

Recognition of the sources of metals and fluids is crucial to determine the genesis of gold deposits, especially in distinguishing the orogenic and magmatic hydrothermal deposits. There is no consensus on the source and genetic style of the Mesozoic gold deposits in the North China Craton (NCC). The Taijiying gold deposit in the Chifeng-Chaoyang gold district on the northern margin of the NCC is a medium-sized gold deposit and worth studying for its sources of metals and fluids. It is hosted by amphibole- to granulite-facies metamorphic rocks and Mesozoic intrusions, and controlled by NNE-, NE-trending compressional reverse faults and NW-trending extensional normal faults. The gold mineralization types include auriferous quartz veins and wall rock alterations of phyllic mineralization, pyritization, chloritization, and carbonatization. According to the crosscutting relationships of the veins and the mineral textures within the ore-bearing veins, four mineralization stages are recognized: clouded-white quartz ± pyrite (stage I), gray quartz + pyrite (stage II), quartz + polymetallic sulfides (stage III), and calcite ± quartz (stage IV), among which the stages II and III represent the main gold mineralization stages. The timing of the gold mineralization is constrained to the Middle Triassic by zircon U-Pb ages of a pre-metallogenic diorite (258.0 ± 1.9 Ma) and a ore-related granitic porphyry dike (241.5 ± 2.2 Ma). Three types of fluid inclusions (FIs) in the quartz veins of four stages are identified: vapor-rich (type 1), CO_2-H_2O three-phase (type 2), and liquid-rich FIs (type 3). Their trapping temperatures gradually decrease from 352 ℃ (stage I) to 124 ℃ (stage IV), with salinities decreasing from 9.8 to 2.0 wt% NaCl eqv., indicating that the ore-forming fluids belong to a H_2O-NaCl-CO_2 system. The first three stages were characterized by moderate-high temperatures, a large variation in salinities, akin to those of the magmatic hydrothermal fluids. The H-O isotope compositions from the stage II ($\delta^{18}Ow$ = 4.1–4.8‰ and δD = -110 to −87‰) to the stage III ($\delta^{18}Ow$ = 3.5 to 3.7‰ and δD = -101 to −98‰), indicate that the ore-forming fluids were mainly magmatic fluids. The $\delta^{34}S_{V\text{-}CDT}$ (1.7–2.1‰), Pb isotopes ($^{206}Pb/^{204}Pb$ = 15.09–15.90, $^{207}Pb/^{204}Pb$ = 15.00–15.15, $^{208}Pb/^{204}Pb$ = 35.76–37.97), and Os isotopes (initial $^{187}Os/^{188}Os$ = 2.3 ± 1.0) of the Au-bearing pyrite samples at the stages II and III, similar to those of the crust-derived magma, suggest that the gold and other metals were extracted from the partial melting of the lower crust. Accordingly, the Taijiying gold deposit is probably a magmatic hydrothermal deposit. The areas recording the Triassic batholith with a developed fault system would be prospective targets for gold mineralization in the Chifeng-Chaoyang district on the northern margin of the NCC.

1. Introduction

As one of the most important Au-bearing deposit types, orogenic gold deposits have attracted intensive investigations in many decades and no consensus has been reached concerning their genesis (Goldfarb and Groves 2015). Most Mesozoic giant gold deposits in the North China Craton (NCC) have been identified as the orogenic gold type, characterize by auriferous quartz veins or wall rock alterations (Miller et al. 1998; Groves et al. 1998; Hart et al. 2002; Chen et al. 2009; Goldfarb et al. 2020). They are hosted in the Precambrian basement and are controlled by faults (Goldfarb et al. 2001, 2005; Hart et al. 2002; Chen et al. 2006; Goldfarb and Groves 2015; Yang et al. 2016; Deng et al. 2017; Groves et al., 2020). Much controversy still exists regarding whether their metal and fluid sources are metamorphic or derived from

* Corresponding authors.
E-mail addresses: yingtong@pku.org.cn (Y. Tong), gaojianfeng@mail.gyig.ac.cn (J.-F. Gao).

https://doi.org/10.1016/j.oregeorev.2021.104593
Received 1 April 2021; Received in revised form 9 November 2021; Accepted 16 November 2021
Available online 20 November 2021

mantle with variable involvements of meteoric water (Powell et al. 1991; Nesbitt 1993; Mao et al. 2003a; Chen et al. 2008; Phillips and Powell 2010; Yang et al. 2016; Liu et al. 2019a). Recently, inputs of magmatic or mantle-derived fluids have been proposed to explain variations in metal contents, isotopic compositions, and mineralogy of individual orogenic gold deposits in the NCC (Robert 2001; Goldfarb et al. 2005; Hammond et al. 2011; McFarlane et al. 2011; Treloar et al. 2015; Spence-Jones et al., 2018). Wang et al. (2019) have highlighted the importance of mantle-derived, Au-bearing hydrous magmas in their origin, whereas a metamorphic fluid source from devolatilization of metasedimentary or metabasic rocks has been proposed for the formation of the majority of the orogenic deposits worldwide or in the NCC (Kerrich, 1989; Goldfarb et al. 1991; Goldfarb et al., 1993; Mccuaig and Kerrich 1998; Large et al. 2007; Phillips and Powell. 2010; Pitcairn et al. 2015; Bark et al. 2020; Li et al., 2020a; Qiu et al. 2020). In contrast, the magmatic hydrothermal deposits have relatively specific features in the sources of fluids and metals.

The Chifeng-Chaoyang gold district represents an important Mesozoic gold mineralization area in the NCC (Fig. 1). Previous work has focused on fluid inclusions and isotopes of the large gold deposits in the district. Some workers have proposed that the majority of the gold deposits were associated with magmatism (Hart et al. 2002). For example, the Dongwujiazi orogenic gold deposit (Early Jurassic) was subjected to a mixture of magmatic and meteoric fluids (Zhang et al. 2009a). The Jinchanggouliang gold deposit (131 Ma) was probably a magmatic-hydrothermal deposit with involvements of magmatic fluids (Liu et al. 2019b), similar to the Anjiayingzi gold deposit (130 Ma), of which the ore-forming fluids, sulfur and metals were related to degassing and devolatilization of Early Cretaceous magmatism (Fu et al. 2016). In contrast, other workers have argued for an orogenic type and suggested that the sulfur- and gold-bearing fluids were generated during retrograde metamorphism, as exemplified by the Shanwanzi and Yuerya gold deposits (Sun 2013; Li et al., 2020b). Therefore, the metal and fluid sources, and the genetic type of the gold deposits in the Chifeng-Chaoyang district remain ambiguous.

The Triassic Taijiying gold deposit in the eastern Chifeng-Chaoyang

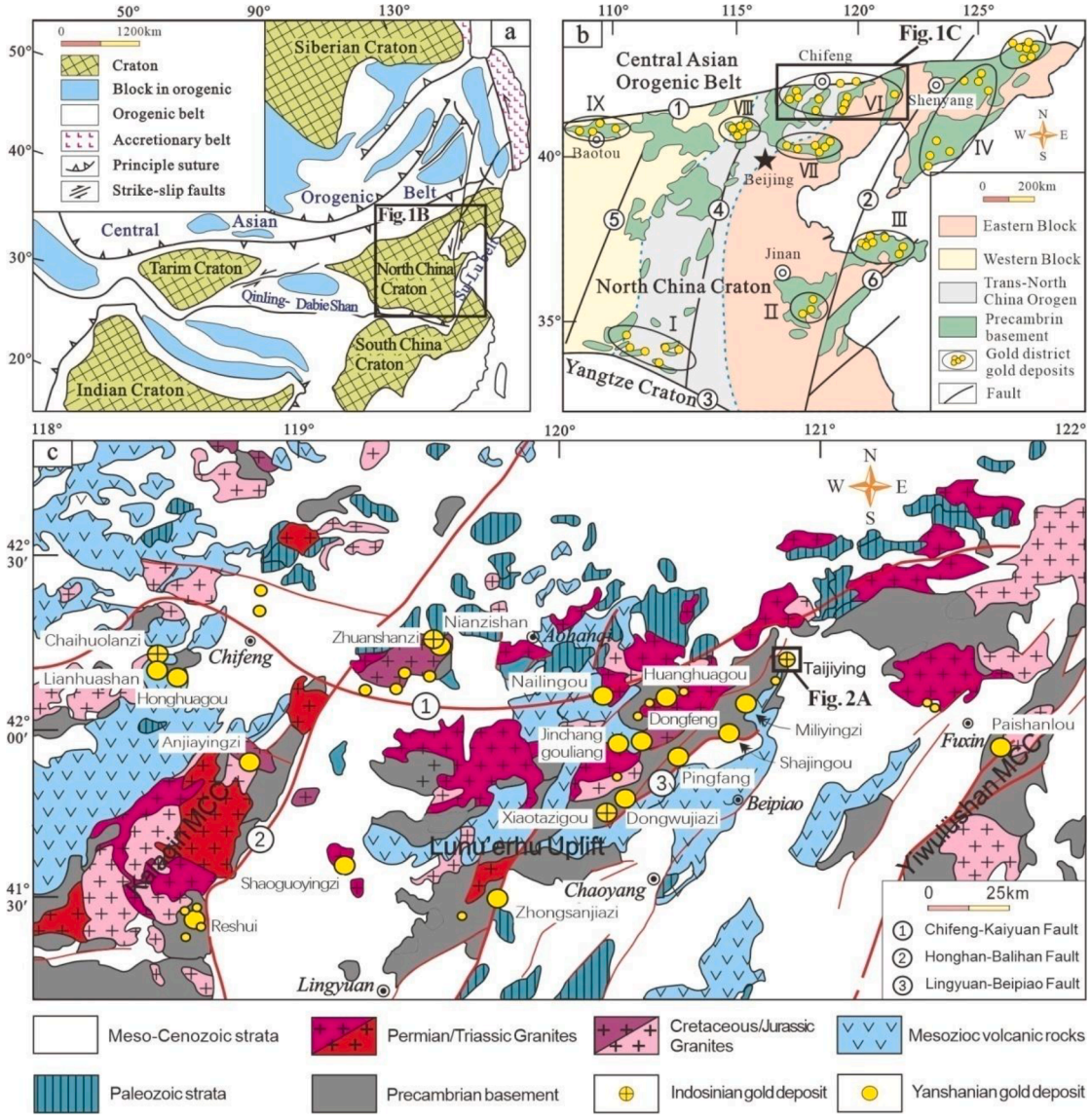

Fig. 1. a, Location of tectonic skeleton map of East Asian and location of the North China Craton(modified from (Zhou and Wilde. 2013). b, Location of gold deposits districts in the North China Craton (Yang et al. 2003); Xiaoqinling-Xiongershan (I), western Shandong(II), Jiaodong Peninsula (III), eastern Liaoning (IV), southern Jilin (V), Chifeng-Chaoyang (VI), eastern Hebei-western Liaoning (VII), Zhang-Xuan (VIII), Daqingshan (IX). Faults: ① Chifeng-Kaiyuan Fault; ② Tan-Lu Fault; ③ Xiaotian-Mozitan Fault; ④ Xingyang-Kaifeng-Shijiangzhuang-Jianping Fault; ⑤ Huashan-Lishi-Datong-Duolun Fault; ⑥ Wulian-Mishan Fault. c, Geological map of the Chifeng-Chaoyang gold district showing distribution of the Mesozoic granites and gold deposits (Yang et al. 2003).

gold district, controlled by northeast- and northwest-trending faults, is hosted in the Xiaotazigou Formation of the Archean Jianping Group and has auriferous quartz veins and alteration of wall rocks. Investigations on the sources of the ore-forming fluids and metals of the Taijiying gold deposit can provide crucial clues to determine the genesis of the early Mesozoic gold deposits in the Chifeng-Chaoyang gold district. In this context, based on detailed field studies, we provide new zircon U-Pb data for the ore-related granitic porphyry and pre-mineralization diorite dike to constrain the timing of metallogeny. Fluid inclusions and H-O isotopes for auriferous quartz and S-Pb-Os isotopes of Au-bearing pyrite are analyzed to examine the features and origin of the ore-forming fluids and metals. New data helps us understand the genesis of the Taijiying gold deposit, shedding lights on locating the prospective gold deposits on the northern margin of the NCC.

2. Regional geology

The triangular NCC with an area of ca. 1,500,000 km^2 is bounded by the Central Asian Orogenic Belt (CAOB) to the north, the Su-Lu UHP belt to the east, the Qilian Orogen to the west and the Qinling-Dabie Orogenic Belt to the south (Fig. 1a). It experienced significant crustal growth at ca. 2.5–2.7 Ga (Zhai and Zhou, 2015). The amalgamation of the Eastern and Western Blocks along the N-S trending Trans-North China Orogen is generally considered to have occurred at ~ 1.85 Ga (Zhai and Zhou, 2015). At ca. 1.32 Ga, tholeiitic diabase sills or dike swarms constitute a Mid-Mesoproterozoic large igneous province in the northern NCC (Zhang and Zhao, 2016). The multiple-stage lithospheric thinning and destruction of the NCC resulted from the intense westward subduction of the Paleo-Pacific oceanic plate during Mesozoic.

The Chifeng-Chaoyang gold district is located on the northern margin of the NCC, adjacent to the CAOB to the north (Fig. 1a and 1b). This district comprises three NE-trending uplift belts, including the Kalaqin and Yiwulüshan metamorphic core complexes (MCCs), and the Lunu'erhu uplift. The district consists mainly of Precambrian basement rocks and Paleozoic to Mesozoic magmatic and sedimentary rocks (Fig. 1c). The Precambrian basement rocks are composed of the Xiaotazigou Formation of the Neoarchean to Paleoproterozoic Jianping Group, which consists of sedimentary and volcanic sequences, and tonalite-trondhjemite-granodiorite (TTG) gneisses with different degrees of migmatization (LBGMR 1989; Liu et al. 2011; Liu et al. 2019b). These rocks were metamorphosed to granulite facies at ca. 2485 Ma and were retrograded to greenschist facies at ca. 2450–2401 Ma (Kröner et al. 1998; Liu et al. 2011; Wang et al. 2011).The Proterozoic and Paleozoic strata of the region consist of thickly bedded limestone and dolomite, which unconformably overlie the Archean basement rocks (Song et al., 2016). Mesozoic volcanic rocks are continental volcanic rocks, which mainly include basalt, basaltic andesite, andesitic breccias, tuff (Fu et al. 2012).

The Permian-Triassic magmatism may have been caused by the final closure of the Paleo-Asian Ocean and the amalgamation between the Mongolian arc terranes and the NCC along the Solonker suture during late Permian to Early Triassic time (Xiao et al. 2003; Zhang et al. 2009b; Zhang et al., 2005c; Zhang et al., 2009d). The Triassic intrusions are mainly distributed in the southern Chifeng City and dominated by granodiorite and alkalic granite, with minor basic and ultrabasic rocks. The Cretaceous magmatic rocks that were attributed to the post-collisional/post-orogenic extension and decratonization of the NCC (Mao et al. 2003b; Chen et al. 2009) mainly formed at 130–120 Ma (Zhang et al., 2014).

The structural framework in this district is dominated by the EW-trending Chifeng-Kaiyuan Fault, the NE-trending Lingyuan-Beipiao Fault, and the NNE-trending Honghan-Balihan Fault (Fig. 1c). The Chifeng-Kaiyuan Fault separates the Hingan-Mongolian orogenic belt (the middle and east parts of the CAOB) from the NCC (Zeng et al. 2011). It had been active since the Proterozoic, as evidenced by a zircon U-Pb age of 1860 Ma for plagioclase amphibolite in the Baoyintu Group (Chen et al. 2015) and had been reactive in the Caledonian and Variscan period. Due to the oblique subduction of the Paleo-Pacific oceanic plate, this fault was re-activated in the Cretaceous along with formation of coeval gold-related intrusions. The left lateral compression-torsion Lingyuan-Beipiao Fault extends from Lingyuan to Beipiao City with a length of more than 200 km, which also formed in the Proterozoic due to the collision between the Siberia Craton and the NCC in the Indosinian. Weakly extensional reactivation in the Early Cretaceous did not change its Jurassic compressional features. The Honghan-Balihan Fault consists of a ~ 3 km-thick ductile and ductile–brittle shear zone passing upward into ~ 100 m-thick brittle chloritic breccia and ~ 0.5 m-thick micro-breccia with fault gouges (Wang and Zheng 2005). It has been active since the Late Jurassic. They divide the study area into several rhombic blocks, where gold deposits and magmatic rocks are exposed (Zhang et al. 2010). Furthermore, the NE-trending Jiguanshan Fault is a compression-torsional normal fault located between the former two faults in the northwestern part of the Taijiying gold field (Fig. 2a). It was thought to have started from the Variscan and been strongly reactivated in the Yanshanian (refs?). This local fault dips to NW with a dip angle of 60° and 50 km in length and plays a significant role in defining the distribution of acidic dikes, subordinate fractures, and gold mineralization.

The Archean metamorphic rocks and Mesozoic granites constituting the three MCCs host many gold deposits (e.g. the Anjiayingzi, Jinchanggouliang, and Paishanlou deposits) related to magma underplating and fluid metasomatism. The chronologic results indicate that the gold metallogenesis occurred at 250–230 Ma, coincident with the post-orogenic extension (Yang and Wu 2009; Zhang et al. 2009b, c, d; Zeng et al. 2011). Those formed at 140–120 Ma were possibly related to the decratonization of the NCC (Shao et al. 1999; Wu and Sun 1999; Zhai et al. 2002).

3. Deposit geology

The medium-sized Taijiying gold deposit owned by the Nanjing Mingda Mining Co., Ltd, is located approximately 9 km northwest of Heichengzi Town and has newly explored gold reserves of 15.1 t with a grade of 11.1 g/t Au, which has not been conducted under official mining yet (Qu et al., 2015; Fig. 2b). The ore bodies are hosted in the Jianping Group, which is bounded by the Chifeng-Kaiyuan Fault to the north, the Jiguanshan Fault to the northwest, and the Lingyuan-Beipiao Fault to the southeast (Fig. 1c).

3.1. Wall rocks and ore-controlling structures

The Archean Jianping Group is the main wall rock of the gold lodes and comprises predominately metamorphic volcanic and sedimentary rocks with a small portion of magnetite quartzite and pyroxene magnetite quartzite (Liu et al. 2011). EW-trending diorite and NE-trending granite porphyry dikes are exposed within the metamorphic basement. The former is crosscut by gold lode I, indicating that the diorite dike is pre-metallogenic. However, the latter is basically parallel to the gold lode I and locally related to it, indicating a close spatial and genetic relationship between the granite porphyry dike with the gold mineralization (Fig. 2b and Fig. 3a).

Most gold lodes are hosted by a series of NNE-trending compressional reverse faults and NW-trending extensional normal faults (Fig. 2 and Table 1). Four NNE- and NE-trending compressional faults show dip angle of 40° to 77° and 146 m to 850 m in length. The longest fault F_1 is characterized by a length of 2 m to 4 m, massive, fragmented, breccia of wall rocks, strong silicification, and weak chloritization (Fig. 4a, b). As the subordinate fractures, two NW-trending extensional faults hosting the gold lodes III to VII are shorter and shallower than the former ones, with a length of 75 m to 340 m and a depth of 100 m to 450 m. Many branches are also observed along the main faults. Extensive quartz veins indicate strong silicification in mineralization (Fig. 4c). The presence of

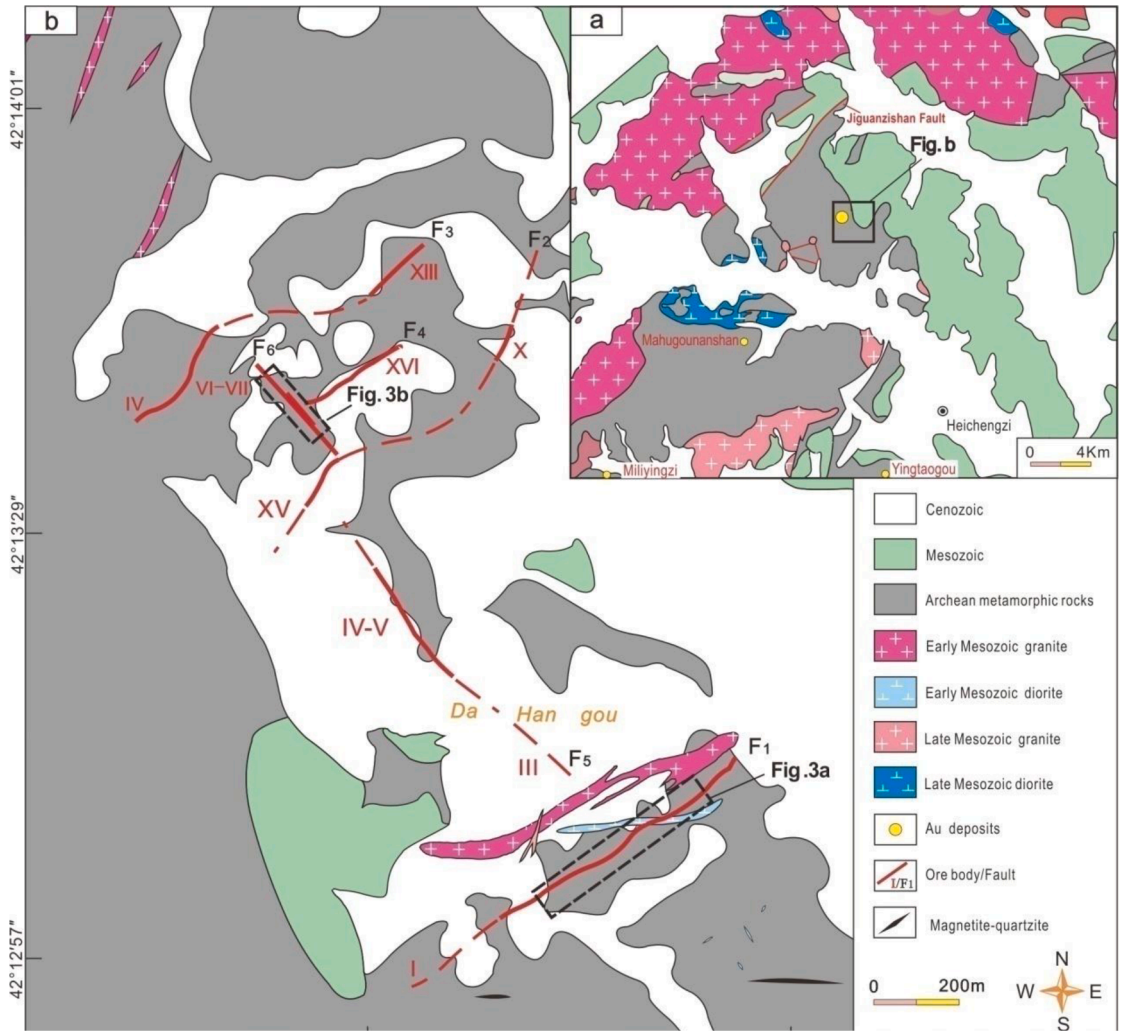

Fig. 2. a, Regional geology of the Taijiying-Mahugou ore field (Revised from 1:200000 regional Geological maps of Xiawa). b, Ore geology of the Taijiying gold deposit.

cataclasite and breccia indicate that these faults experienced brittle deformation.

3.2. Ore bodies

Ore lodes are partially covered by Quaternary and Cretaceous volcanic tuff. Ten economic lodes have been identified with a thickness of 0.7 m to 1.8 m, a length of hundreds of meters, and a dip angle of 40° to 80° (Table 2). The primary lode I is controlled by compressional faults F_1 with a large depth and few branches. This lode shows a dip direction of 320° to 330° and a dip angle of 40° to 76°. The scale revealed by drilling holes are 850 m in length and 650 m in depth with an average thickness of 1.02 m and an average grade of 11.49 g/t. The distribution of high grade zone is consistent with that of granite porphyry dike, especially the contact zone. On the contrary, the secondary important lode VI is defined by the extensional faults with a smaller scale (280 m in length and 300 m in depth) and more branches (Fig. 3). Lode VI is nearly perpendicular to the former one with a dip direction of 215° to 220° and a dip angle of 63° to 66°. Its width ranges from 0.77 m to 0.85 m and grade varies from 10.28 g/t to 12.22 g/t. The mineralization types are wall rock alteration and/or quartz vein types (Fig. 3 and Fig. 4d-4i).

3.3. Mineralization and alteration

The wall rock alterations occur near the ore bodies and include silicification, sericitization, pyritization, chloritization, and carbonatization (Fig. 5). The pyritization is closely related to gold mineralization, the degree of which depends on the features of pyrites, such as grains, color, and crystallinity. For example, the black fine-grained anhedral pyrites usually indicate a higher grade of Au than the pale yellow coarse-grained euhedral pyrites (Fig. 6a, b, h, i). Carbonatization is characterized by euhedral to subhedral carbonate minerals (calcite) in the veinlets (0.5–5 mm), suggesting the end of mineralization.

The ore minerals are predominantly pyrite with minor pyrrhotite (locally altered to limonite), native gold, electrum, galena, sphalerite, and chalcopyrite (Fig. 6). The gangue minerals are dominated by quartz, chlorite, sericite, and calcite. Native gold with sizes of 10–80 μm occurs as rounded grains, breccia, branches, flakes, emulsions, or irregularly shaped fine grains within intergranular spaces and filling fissures. Some gold grains occur as irregular inclusions within pyrite and chalcopyrite (Fig. 6). Ore structures are mainly massive, veinlet, and disseminated, and locally banded and brecciated (Fig. 4d-4i).

Based on field observations, mineral assemblages, and crosscutting relationships, the mineralization can be divided into four stages: (I) clouded-white quartz ± pyrite; (II) gray quartz + pyrite; (III) quartz + polymetallic sulfides; and (IV) calcite ± quartz (Fig. 7). Stage I is characterized by clouded-white barren quartz veins with minor pyrites. stage II is the main gold mineralization stage, defined by fine-grained anhedral pyrite (py II) with disseminated gold and a small amount of electrum. Stage III shows weak gold mineralization and is marked by the

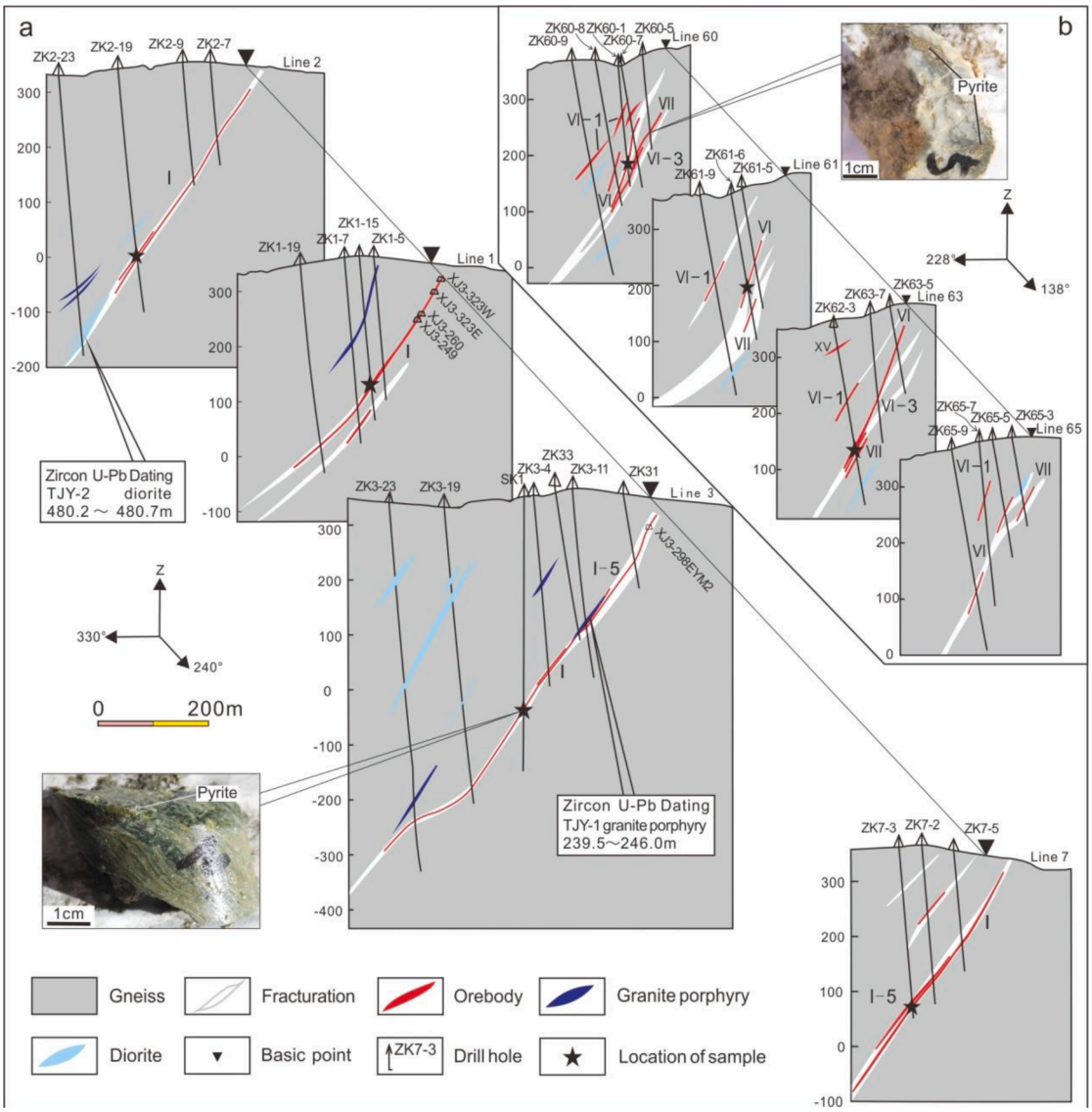

Fig. 3. The image of combined profile from ore bodies. a, Line 2 to 7 of orebody I with the less branches and deep-seated metallogeny controlled by strike–slip compressive fault. b, Line 60 to 65 of orebody VI with more branches and shallower metallogeny controlled by extensional fault.

presence of sulfides, such as pyrite (py III), chalcopyrite, galena, and sphalerite. Stage IV is represented by calcite and quartz, reflecting the end of gold mineralization.

3.4. Samplings and methods

Samples TJY-1 (granitic porphyry) and TJY-2 (diorite) were collected for laser ablation inductively coupled plasma mass spectrometry (LA-ICP-MS) zircon U-Pb dating. The sampling locations are shown in Fig. 3. Representative gold ore samples were selected from different stages for fluid inclusion and H-O isotopic analyses, and Au-bearing pyrites were selected for S, Pb, and Re-Os isotopic analyses. The methods are detailed in the supplementary material ESM_1.

4. Results

4.1. Zircon U-Pb dating

Granitic porphyry (TJY-1): Zircons are mostly euhedral, columnar, and colorless with a length of 120–180 μm and a width of 60–130 μm. The analyzed grains exhibit oscillatory growth zoning (Fig. 8a) and have high Th/U ratios (0.44–1.01) (Appendix A). Their U and Th concentrations are 419–1747 ppm and 184–1603 ppm, respectively, and exhibit a positive correlation, reflecting their magmatic origin (Belousova et al. 2002; Hoskin and Schaltegger 2003). 15 analyzed spots cluster on the concordia line (Fig. 8a) and yield a weighted mean $^{206}Pb/^{238}U$ age of 242 ± 2 Ma (MSWD = 2.5).

Diorite (TJY-2): Zircons are mostly euhedral columnar and colorless with a length of 70–140 μm and a width of 30–70 μm. The analyzed grains have clear oscillatory growth zoning (Fig. 8b), low U (37–91 ppm), high Th concentrations (74–222 ppm), a positive correlation between U and Th, and high Th/U ratios (1.14–2.23), which reflect their magmatic origin (Appendix A; Belousova et al. 2002; Hoskin and Schaltegger 2003). 10 spots cluster closely on the concordia line (Fig. 8b), yielding a weighted mean $^{206}Pb/^{238}U$ age of 258 ± 2 Ma (MSWD = 0.7).

4.2. Fluid inclusions

4.2.1. Petrography

Quartz represents the host mineral of the fluid inclusions at the four stages. There are late secondary fluid inclusion trails in the gold

Table 1
The features of main faults in Taijiying gold deposit.

No.	Ore body No.	Attitude (°) Trending	Dip	Length(m) Trending	Dip	Attribute	Features
F_1	I	NEE (Wavy)	NW, 40 ~ 70	850±	370 ~ 650	Sinistral rotation, Compression-torsion fault	2–4 m in width with massive, fragmented, breccia of wall rock; strong silicification and moderate chloritization; shear joint developed; compound of branch; The granite porphyry was crosscutted by fracture belt.
F_2	X	NE	NW, 50 ~ 77	531±	200 ~ 486		1–18 m in width with gentle dip angles in the north and steep ones in the south
	XV	NE	NW, 55 ~ 60	123±	210 ~ 290		1–18 m in width and dislocation with 3 m displacement at the level of + 300 m.
F_3	IX	NE	NW, 40 ~ 50	146±	264		2–5 m in width, cataclasite with weak chloritization, silicification, and pyritization were filled by the siliceous, carbonate, and argillaceous
	X III	NE	NWW,43 ~ 56	200±			2–5 m in width
F_4	XVI	NE	NW, 52 ~ 58	190±	129 ~ 198		2–7 m in width
F_5	III	NW	SW, 56 ~ 70	75±	230 ~ 240	extension fault	2–3 m in width with cracks. Strong silicification developed in the north and chloritization in the south.
	IV	NW	SW, 57 ~ 85	294±	100 ~ 230		4–27 m in width, cataclasite with strong chloritization and silicification.
	V	NW	SW, 57 ~ 86	280±	200 ~ 290		2–8 m in width, altered cataclasite with weak silicification and kaolinization
F_6	VI	NW	SW, 50 ~ 75	340±	150 ~ 400		2–10 m in width, altered cataclasite with strong pyritization
	VII	NW	SW, 48 ~ 79	325±	130 ~ 450		6–50 m in width, cataclasite with weak chloritization and pyritization were filled by silicification, argillaceous

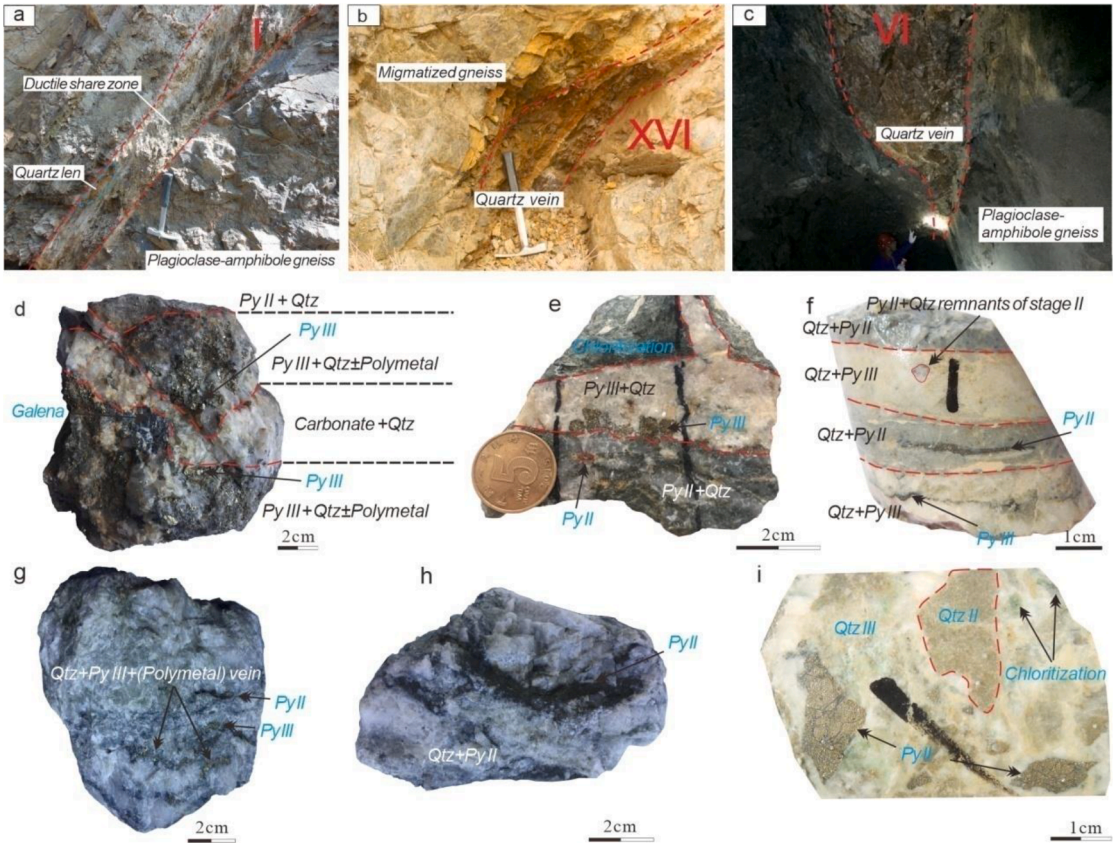

Fig. 4. Orebodies outcrops and ore photographs showing vein mineralization paragenesis in Taijiying gold deposit. a–c, orebodies outcrops in the Taijiying gold deposit. d, Fine-grain pyrites and gray quartz (PyII + Qz) of stage II was crosscut by coarse-grained euhedral pyrites, galena and milky white quartz vein (PyIII + Qz ± Polymetal) of stage III, Carbonate + Qz vein can be seen from stage IV. e, Chloritic wall rock was crosscut by Qz + PyII of stage II, which was then intruded by Qz + PyIII of stage III. f, Gray Qz with banded PyII crosscut by Qz + PyIII. g Qz + PyIII + Polymetallic sulfide vein intrude veins of the stage II. h, Qz + PyII from stage II. i, Qz from stage III of VI lode contains brecciated Qz + PyII. Abbreviations: Qz, quartz; Py, pyrite; and Gn, galena.

Table 2
The main features of the orebodies from the Taijiying gold deposit.

Ore body No.	Dip direction (°)	Dip angle (°)	Length (m)	Depth (m)	Average thickness (m)	Average grade(g/t)
I	320 ~ 330	40 ~ 76	850	650	1.02	11.49
III	233	64	80	240	0.69	36.19
IV	238	52 ~ 78	135	100	1.20	11.83
V	238	52 ~ 78	280	193	0.88	2.50
VI	215 ~ 220	66	230	300	0.77	12.22
VII	215 ~ 220	63	280	310	0.85	10.28
VI-1	215 ~ 220	65	180	250	1.21	4.23
X	305	66 ~ 80	190	250	0.84	7.52
X-1	305	66 ~ 81	155	130	1.79	10.13
XVI	330	53	180	140	0.72	6.17

deposits, but secondary CO_2-H_2O fluid inclusion trails cutting through primary fluid inclusions were not observed in Fig. 9. All fluid inclusions (FIs) in this study were treated as primary FIs. Based on the components and phase transition characteristics of the inclusions at room temperature, three types of FIs are identified in the Taijiying gold deposit (Fig. 9): type 1 FIs (vapor-rich inclusions) (Fig. 9b), type 2 FIs (CO_2-H_2O three-phase inclusions) (Fig. 9a-d), and type 3 FIs (liquid-rich inclusions) (Fig. 9c, d, g).

Type 1 FIs: these inclusions consist of a liquid phase and a vapor bubble with vapor bubbles occupying 60–85 vol%. They are mainly 3–8 μm in diameter with irregular and oval shapes. These inclusions homogenize to the vapor phase when heated. They commonly appear as clusters with the type 2 FIs in the stages I-III (Fig. 9a, c, e).

Type 2 FIs: these inclusions consist of aqueous and two carbonic phases (Figs. 9a-d, f). They have generally irregular and oval shapes with a diameter of 3 μm to 13 μm and bubbles occupying 40–80 vol%. These inclusions are the most common type of inclusions at all paragenetic stages, accounting for approximately 45% of the total inclusions. They coexist with the types 1 and 3 FIs as clusters or scattered forms.

Type 3 FIs: these inclusions are mainly 2 μm to 12 μm in diameter with oval, rounded, irregular, and negative crystal shapes (Fig. 9b, c, d, g). Most vapor–liquid ratios are 5–35 vol%. This type of FIs accounts for approximately 35% of the total inclusions and often coexists with the type 2 FIs as clusters or scattered forms. These FIs are distributed in groups or as individual in quartz at all stages.

The FIs in quartz at the stage I consist of the types 1 and 2, which are mainly 4–10 μm in diameter and have irregular, oval, and negative crystal shapes with most vapor–liquid ratios of 45–85 vol%. Most FIs are present as clusters or isolated ones, indicating a primary origin. The three types of FIs at the stage II are mainly 3–12 μm in diameter with vapor–liquid ratios of 10–80 vol% and scattered or in groups with irregular to negative crystal shapes. The FIs at this stage contain abundant type 2 inclusions with subordinate types 1 and 3, accounting for 60%, 25%, and 15% of the total inclusions, respectively. All types of FIs are observed in quartz at the stage III with an increasing volume of the type 3 inclusions (40%). The type 1 and 2 FIs decrease to 15% and 45%, respectively. These FIs are also scattered or in groups with irregular to negative crystal shapes. The type 3 FIs (2 μm to 12 μm, mostly 8 μm) are much larger than those at the stage II. The type 3 FIs are the major FIs at the stage IV, accounting for approximately 75% of the FIs with various sizes from 2 to 11 μm in diameter. These inclusions appear as clusters or isolated ones with oval or irregular shapes. The vapor–liquid ratios range from 5 vol% to 30 vol%.

4.2.2. *Fluid inclusion microthermometry and Raman spectroscopy*

Microthermometric analysis was conducted on the primary FIs in quartz from all stages. The ore-related aqueous-carbonic inclusions have formed clathrate and some of the water have been frozen in clathrate when the ice melts. Thus, the water, in which the ice melting is measured, is uncharacteristically concentrated in salt. Salinities have been calculated from the clathrate melting temperatures for the aqueous-carbonic inclusions. The data for the FIs in this study are listed in Table 3 and illustrated in Fig. 10a.

The type 1 FIs at the stages I to III homogenize to the vapor state, and the homogenization temperatures ($T_{h,\ total}$) are variable, from 317 to 352℃ (an average of 333℃), 308–321℃ (an average of 315℃), to 243–282℃ (an average of 272℃), respectively. The final ice melting

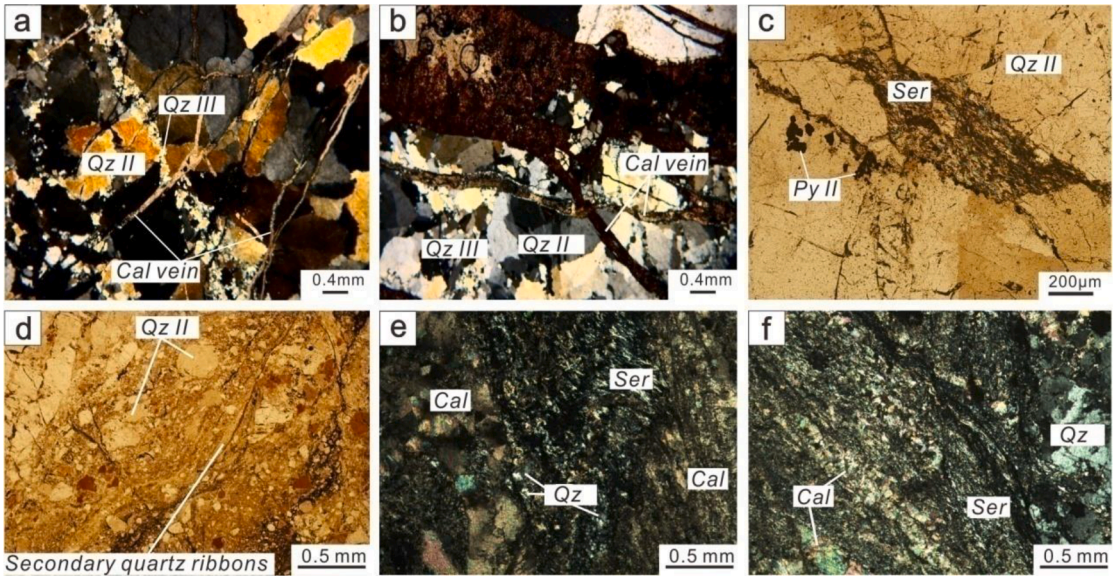

Fig. 5. Photomicrographs of hydrothermal alteration features. a–b, Quartz veinlets from stage III (Qz III) fill fractures within early Quartz (Qz II) or cut the crystal, which are cut by calcite veinlets from stage IV. c, Pyritization, sericitization and silicification, sericite appears as veinlets filling fractures. d, Recrystallized quartz observed as narrow undulated quartz ribbons surrounding the early stage quartz breccia. e–f, Carbonation, carbonate minerals (calcite) exist as vein with sericite and late-stage quartz. Abbreviations: Cal = calcite, Qz = quartz, Ser = sericite, Py = pyrite.

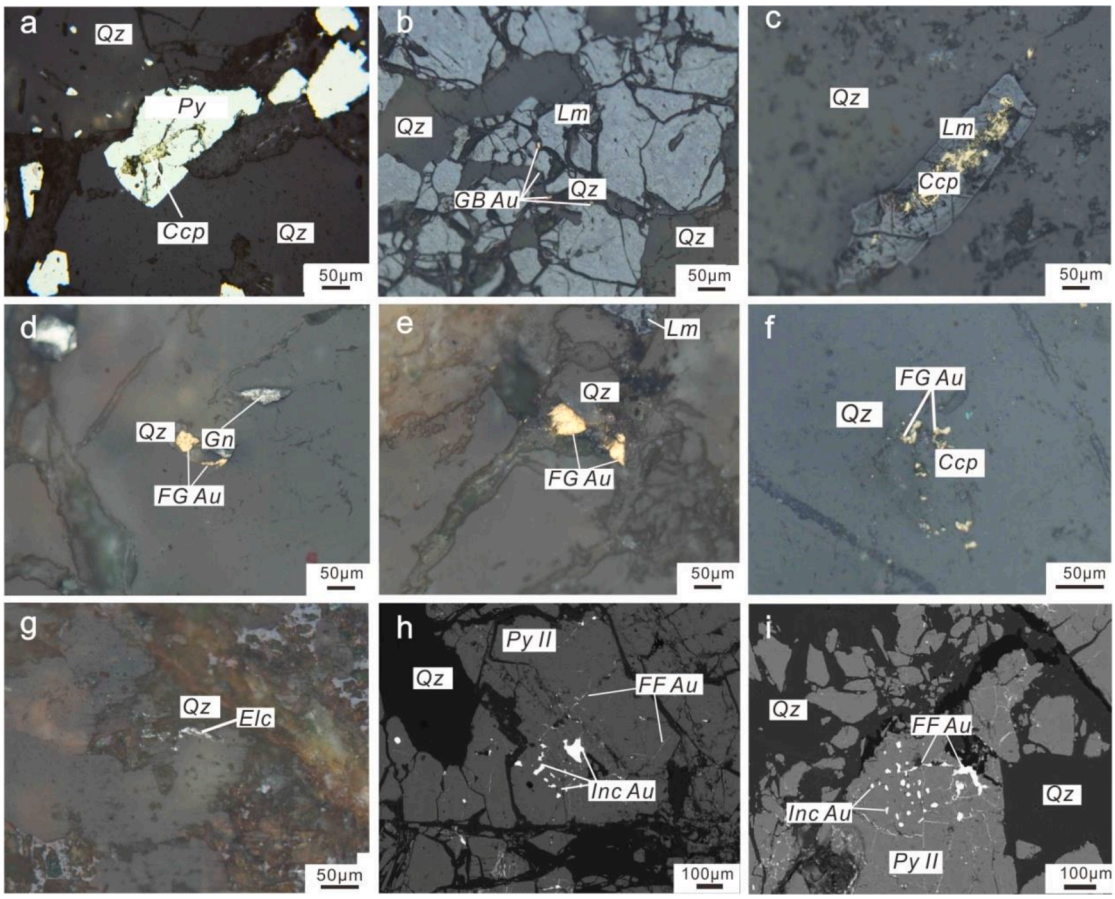

Fig. 6. Photomicrographs (a–g) and BSE (h–i) of gold-related ore samples from the Taijiying gold deposit. a, Pyrite partially being replaced by chalcopyrite. b, Gold grains occur along limonite or quartz grain boundaries. c, Chalcopyrite being dissolved by limonite. d, Gold grains are intergrown with galena (Gn) in quartz. e–g, Quartz vein contains fine native gold grains or electrum. h–i, Gold grains hosted as inclusions or in fractures in Py II. Abbreviations: Ccp, Chalcopyrite; Gn, galena; Py, pyrite; Qz, quartz; Lm, Limonite; Elc, Electrum; FF Au, fracture-fill gold; FG Au, free grains of gold; GB, grain-boundary gold; Inc Au, gold formed as inclusions.

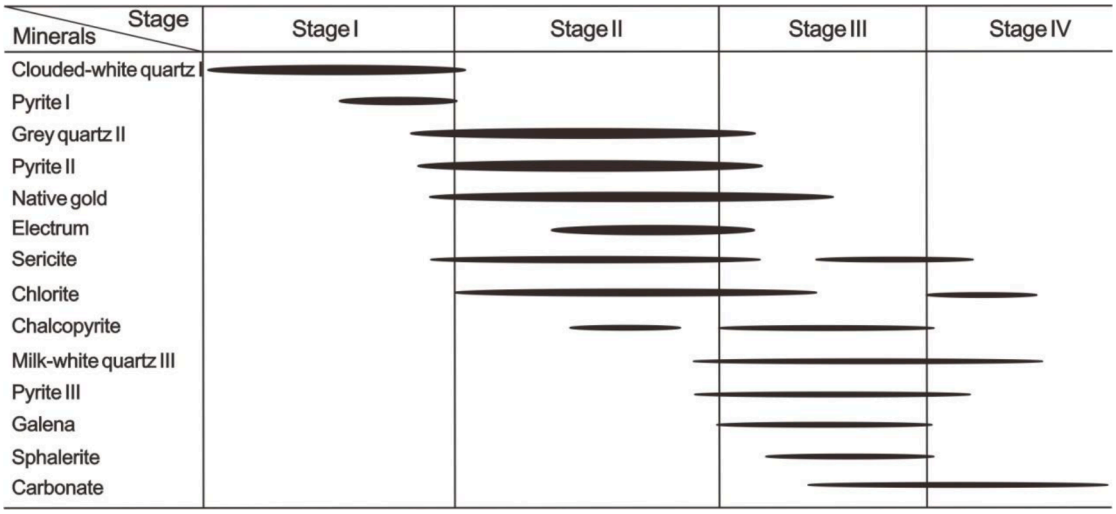

Fig. 7. Paragenesis sequence of ore, gangue, and alteration minerals of the Taijiying gold deposit.

temperatures ($T_{m,\ ice}$) are −4.9 to −5.9 ℃, −3.6 ℃, and −3.4 to −4.2 ℃, respectively, yielding the salinities of 7.7–9.1 wt% NaCl eqv (average 8.4 wt% NaCl eqv), 5.9 wt% NaCl eqv, and 5.5–6.7 wt% NaCl eq (average 6.0 wt% NaCl eqv), respectively.

The type 2 FIs at the stages I to III homogenize to the liquid state, and the $T_{h,\ CO2}$ values vary in a narrow range of 23.7–30.2 ℃ (an average of 29.6 ℃), 23.3–31.1 ℃ (an average of 27.9 ℃), and 22.7–30.9 ℃ (an average of 26.4 ℃), respectively. The homogenization temperatures ($T_{h,\ total}$) are mainly 285–334 ℃ (average 322 ℃), 276–337 ℃ (average 308 ℃), and 265–329 ℃ (average 290 ℃), respectively. The final clathrate melting temperatures ($T_{m,cal}$) of 5.2–6.3 ℃, 6.1–9.0 ℃, 4.5–7.9 ℃ yield the salinities of 7.0–8.7 wt% NaCl eqv (average 7.9 wt% NaCl eqv),

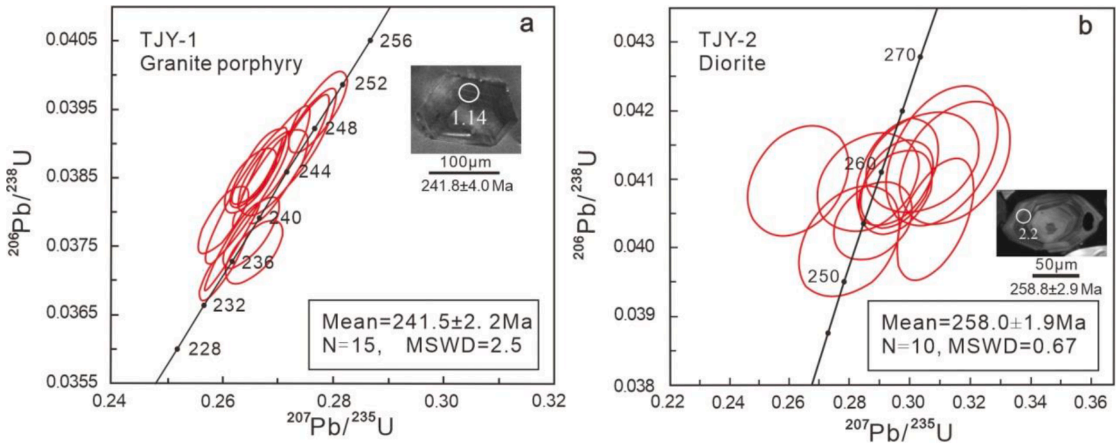

Fig. 8. Plots of LA-ICP-MS zircon U-Pb age for intrusions in the Taijiying gold mine. a, Sample granite porphyry (TJY-1). b, Sample diorite (TJY-2).

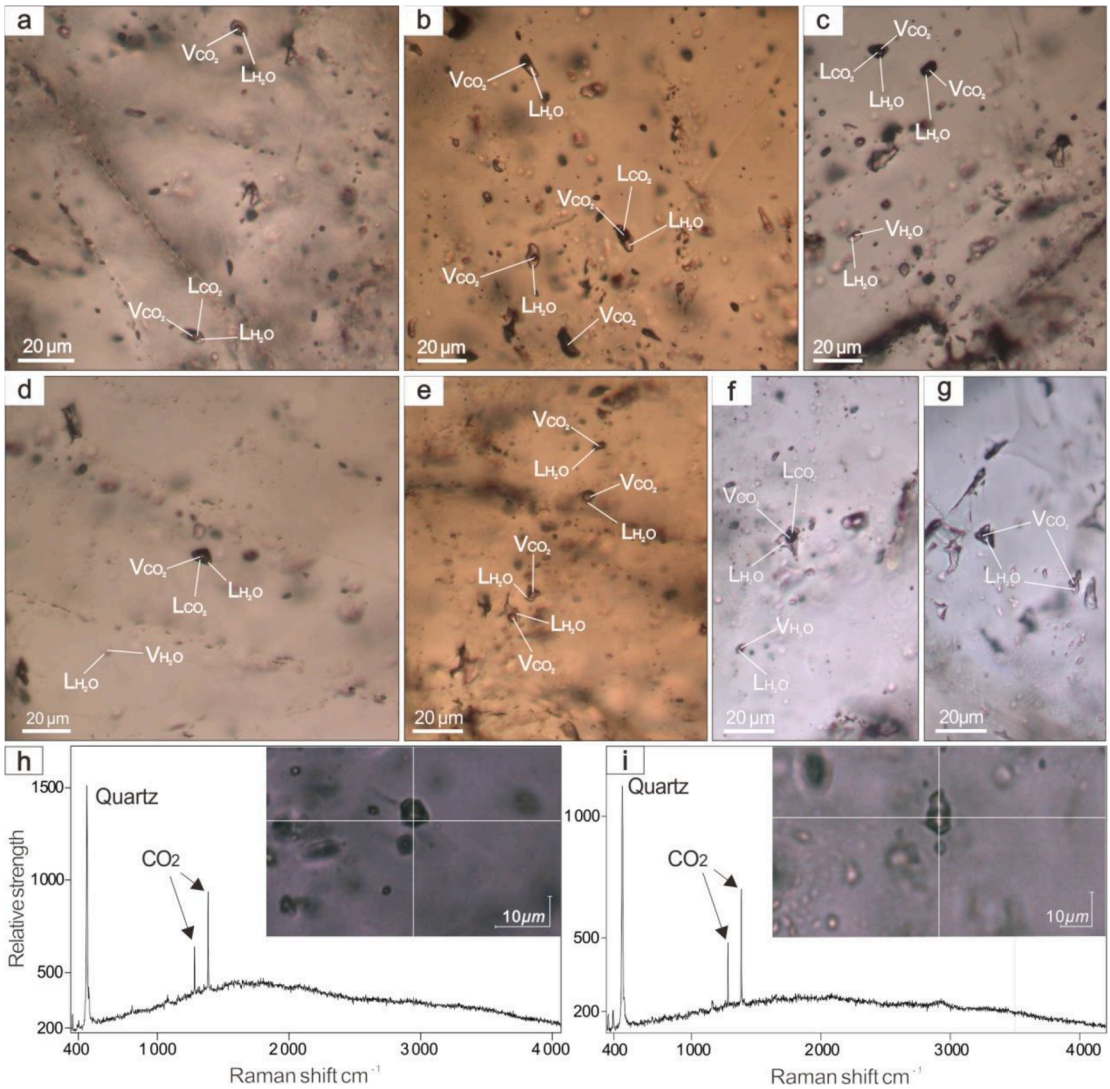

Fig. 9. Transmitted light photographs of fluid inclusions. a, Type 1 vapor-rich inclusion. b, Type 2a two-phase H2O-CO2-NaCl inclusion. c, Type 2b three-phase H2O-CO2-NaCl inclusion. d, Type 3 two-phase H2O-NaCl inclusion. e, Type 1, type 2a and Type 3 inclusions distributed in stage II quartz. f, Type 2a inclusions in stage II quartz. g, Two various fluid inclusion types (Type 2a and Type 3) occurred in stage III quartz. h–i, CO2 peaks on the Raman spectra of the studied vapour phase.

2.0–7.3 wt% NaCl eqv (average 5.4 wt% NaCl eqv), and 4.2–9.8 wt% NaCl eqv (average 7.2 wt% NaCl eqv), respectively. The pressures vary in the range of 137–275 MPa (average 221 MPa for stage I), 140–244 MPa (average 203 MPa for stage II), and 128–269 MPa (average 179 MPa for stage III), which were calculated from the homogenization temperatures of the three-phase inclusions by using the FLINCOR

Table 3
The characteristics of fluid inclusions of quartz from gold ores at Taijiying gold deposit.

Stage	FI type	No.	Size (μm)	Vapor/liquid ratio(vol %)	$T_{h,\ total}$(℃)	$T_{m,\ ice}$(℃)	$T_{m,\ cla}$(℃)	$T_{h,\ CO2}$(℃)	Salinity(wt%NaCl eqv.)	Pressure(Mpa)
I	Type 1	13	4 ~ 8	65 ~ 85/**70**	317 ~ 352/**333**	−4.9 ~ -5.9/-**5.4**			7.7 ~ 9.1/**8.4**	
	Type 2	17	4 ~ 10	45 ~ 80/**52**	285 ~ 334/**322**		5.2–6.3/**5.7**	23.7 ~ 30.2/**29.6**	7.0 ~ 8.7/**7.9**	137 ~ 275/**221**
II	Type 1	2	3 ~ 6	75 ~ 80/**80**	308 ~ 321/**315**	**−3.6**			**5.9**	
	Type 2	19	4 ~ 12	40 ~ 80/**60**	276 ~ 337/**308**		6.1–9.0/**7.1**	23.3 ~ 31.1/**27.9**	2.0 ~ 7.3/**5.4**	140 ~ 244/**203**
	Type 3	9	3 ~ 6	10 ~ 35/**21**	220 ~ 317/**283**	−2.6 ~ -4.0/-**3.6**			4.3 ~ 6.5/**5.8**	
III	Type 1	7	3 ~ 7	60 ~ 80/**71**	243 ~ 282/**272**	−3.4 ~ -4.2/-**3.7**			5.5 ~ 6.7/**6.0**	
	Type 2	24	3 ~ 13	40 ~ 85/**66**	265 ~ 329/**290**		4.5–7.9/**6.1**	22.7 ~ 30.9/**26.4**	4.2 ~ 9.8/**7.2**	128 ~ 269/**179**
	Type 3	14	4 ~ 12	10 ~ 30/**22**	228 ~ 320/**250**	−2.8 ~ -3.7/-**3.4**			4.6 ~ 6.0/**5.5**	
IV	Type 3	18	2 ~ 11	5 ~ 30/**18**	124 ~ 223/**175**	−1.3 ~ -3.6/-**2.4**			2.2 ~ 5.8/**4.0**	

Note: Abbreviations: FI = fluid inclusion, $T_{h,\ total}$ = Total homogenization temperature, $T_{h,\ CO2}$ = homogenization temperature of the CO_2 phases, $T_{m,\ cla}$ = temperature of final clathrate melting. Salinity is calculated according the equation: $w_{NaCl} = -1.78T_{m,ice} - 0.0442T_{m,ice}^2 - 0.000557T_{m,\ ice}^3$ and $w_{NaCl} = 15.52022 - 1.02342T_{m,\ cla} - 0.05286T_{m,\ cla}^2$. The pressure is calculated according to homogenization temperature of three-phase inclusions by FLINCOR. [a] Range/average.
The numbers of bold are the average values.

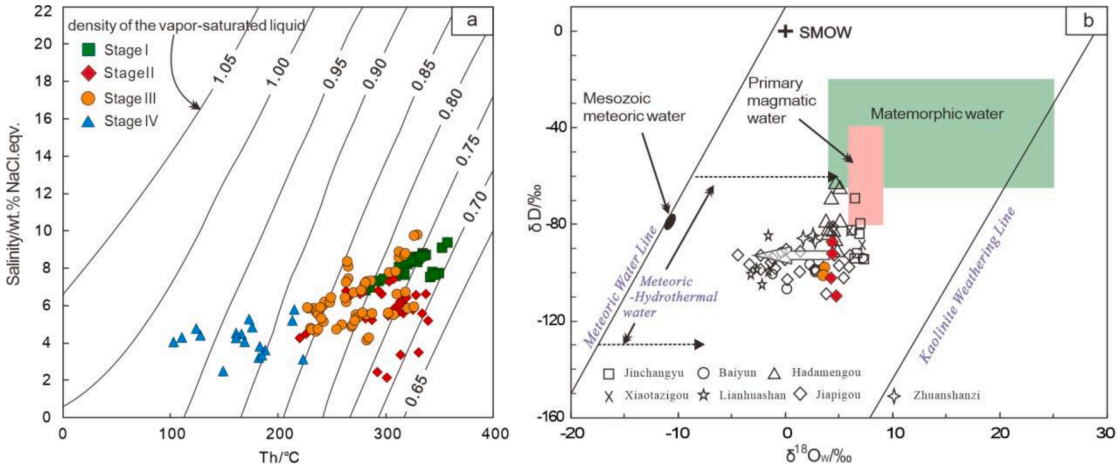

Fig. 10. a, Homogenization temperature (Th) versus salinity plot for the fluid inclusions from the Taijiying gold deposit. b, Plot of δD vs. δ18Ow for ore-forming fluids of the Taijiying gold deposit. Magmatic water, Mantle juvenile water and metamorphic water fields after Taylor, H P. (1974) and Sheppard (1986). Data of Lianhuashan, Xiaotazigou gold deposits are from Sun et al. (2015) and Piao et al. (2007); Data of Hadamengou are from Hou (2011); Data of jinchangyu are from Xiong et al. (2017); Data of Jiapigou are from Yang et al. (2013); Data of Baiyun are from Liu et al. (2019).

software (Brown, 1989).

The type 3 FIs at the stages II to IV homogenize to the liquid state, and the $T_{h,\ total}$ values are 220–317 ℃ (average 283 ℃), 228–320 ℃ (average 250 ℃), and 124–223 ℃ (average 175 ℃), respectively. The final ice melting temperatures ($T_{m,ice}$) of −2.6 to −4.0 ℃, −2.8 to −3.7 ℃ ,and −1.3 to −3.6 ℃ corresponds to the salinities of 4.3–6.5 wt% NaCl eqv (average 5.8 wt% NaCl eqv), 4.6–6.0 wt% NaCl eqv (average 5.5 wt% NaCl eqv), and 2.2–5.8 wt% NaCl eqv (average 4.0 wt% NaCl eqv), respectively.

The results of representative laser Raman spectroscopic analyses are shown in Fig. 9. The gas component of the type 1 FIs at the stage II is mainly CO_2 (Fig. 9i). The liquid component of the type 2 at the stage III and that at the stage IV is confirmed to CO_2 (Fig. 9h). The results of the fluid inclusion microthermometry and laser Raman spectroscopic analyses suggest that the ore-forming fluids generally belong to a H_2O-NaCl-CO_2 system.

4.2.3. Trapping pressure and mineralization depth

The H_2O-CO_2 three-phase inclusions, which are not only common during fluid immiscibility or phase separation, but also need no pressure correction, are used to estimate the trapping pressures in this study. The trapping pressure estimation can be performed since an independent entrapment temperature is known (Brown and Hagemann 1995). The type 2 FIs at the first three stages are used to estimate the trapping pressures by using the FLINCOR program and the formula for the H_2O-CO_2-NaCl system (Brown and Lamb 1989). The trapping temperatures of the stages I to III are 285–334 ℃, 276–337 ℃, and 265–329 ℃, which yield the trapping pressures of 137–275 MPa, 140–244 MPa, and 128–269 MPa, respectively (Table 3).

The characteristics of the mixed brittle-ductile ore-forming structures (Fig. 4) and the pressure fluctuations in the Taijiying deposit imply a fault-valve mechanism (Sibson et al. 1988). The fault-valve model for shear zone-controlled deposits proposes a cyclic fluid pressure fluctuation from lithostatic to hydrostatic due to the episodic tectonic activities in the shear zone. The trapping pressures of the FIs are generally

considered to represent (supra)-lithostatic systems when the fluid pressures were over 40 MPa (Sibson et al. 1988). According to the function ($h = p/\rho g$, p is the homogeneous pressure, ρ is the density, and $g = 9.8\ N/m^2$), the minimum pressures estimated for the main stages II to III correspond to a depth of ~ 5 km. The maximum pressures estimated for the two stages correspond to a mineralization depth of ~ 9 km, given that the density of the overlying Jianping Group is ~ 2.85 g/cm^3. Accordingly, we infer that the gold mineralization in Taijiying mainly occurred at depths of 5–9 km, consistent with the Dongfeng gold deposits (Wen et al. 2015). The Taijiying gold deposit is slightly deeper than most deposits in the Chifeng-Chaoyang district, e.g., Jinchangyu (4–8 km), Xiaotazigou (1.6–2.8 km), Zhuanshanzi (1.2–3.3 km), Jinchanggouliang (2.6–7.1 km), Dongwujiazi (5.1–5.4 km), and Anjiayingzi (5.1–10.1 km) (Fu et al. 2020).

4.3. Oxygen and hydrogen isotopes

The oxygen and hydrogen isotope compositions of 6 quartz samples from the main ore-forming stages II and III are presented in Table 4 and Fig. 10b. The measured $\delta^{18}O_{quartz}$ values of quartz at the two stages range from 10.9 to 11.6‰ and 11.5–11.7‰, respectively. According to the quartz-water fractionation equation ($1000 \times \ln\alpha_{quartz\text{-}water} = 3.38 \times 10^6 \times T^{-2} - 3.40$, Clayton and Bloomquist 1973) and the homogenization temperatures calculated from the fluid inclusion data, the oxygen isotope compositions of the ore-forming fluids can be calculated from the oxygen isotope compositions of quartz. The $\delta^{18}Ow$ values of the two mineralization stages II and III are 4.1–4.8‰ and 3.5–3.7‰, respectively. The corresponding δD values of the fluid inclusion water in quartz are −110‰ to −87‰ and −101‰ to −98‰, respectively.

4.4. S, Pb, and Re-Os isotopes

The sulfur and lead isotopic compositions of ten pyrite samples from the stages II and III are listed in Table 5. The $\delta^{34}S$ values of the ten pyrite samples show a narrow range (+1.7 ‰ to + 2.1 ‰), with an average $\delta^{34}S$ value of + 1.9 ‰. Lead isotope compositions consist of $^{206}Pb/^{204}Pb$ = 18.175–18.422 (an average of 18.262), $^{207}Pb/^{204}Pb$ = 15.572–15.619 (an average of 15.597), and $^{208}Pb/^{204}Pb$ = 35.758–37.970 (an average of 38.180). The μ (μ = $^{238}U/^{204}Pb$) values for the samples at the stages II and III are 9.01–9.44 and 8.98–9.09, respectively. Blank-corrected Re and Os data for the five pyrite samples from the Taijiying Au deposit is given in Table 6. The five samples contain 0.76–15.14 ppb Re and 0.01–0.07 ppb Os. The common Os and ^{187}Os contents are 0.00371–0.0256 ppb and 0.00600–0.0564 ppb, respectively. $^{187}Re/^{188}Os$ ratios range from 160.6 to 6259, and $^{187}Os/^{188}Os$ ratios range from 3.251 to 37.08. The Re-Os isochron age of the five pyrite samples gives 335 ± 19 Ma (MSWD = 61) with an initial $^{187}Os/^{188}Os$ ratio of 2.3 ± 1.0.

Table 4
Oxygen and hydrogen isotopic compositions of fluid inclusion from the Taijiying gold deposit.

Mineralization stage	Mineral	T_h (℃)	$\delta^{18}O_{quartz}$(‰)	$\delta^{18}O_W$(‰)	δD (‰)
II	Quartz	300	11.3	4.5	−92
			11.6	4.8	−110
			11.2	4.4	−87
			10.9	4.1	−102
III	Quartz	270	11.5	3.5	−101
			11.7	3.7	−98

Note: T_h is the average homogenization temperature of every stage; the **δ**^{18}Ow values were calculated according to the quartz-water equilibrium temperature formula provided by Clayton et al., 1972.

5. Discussion

5.1. Timing of gold mineralization

Although the Re-Os isochron age of pyrite (335 ± 19 Ma) has been obtained, they can not be used to constrain the ore-forming age because it is not consistent with geological evidences. The mineralization timing of the Taijiying gold deposit still lacks accurate isotopic dating, but the pre-metallogenic diorite and ore-related granitic porphyry can provide robust age constraints. The diorite dike with age of ca. 258 Ma was cut through by orebody I, which provide the upper limit of mineralization age. All faults in the deposit have not penetrate the Cretaceous strata with the age of 133.6 Ma (Chen et al., 2015). It is can be considered as the lower limit of mineralization age. It seems like that the mineralization of Taijiying occurred during Triassic and Jurassic. However, the Jurassic dikes have not been identified in this field. The Middle Triassic granite porphyry almost parallel to the orebody I (Fig. 2b), indicating their temporal consistency. It is also clear that the granite porphyry dikes are closely associated with the gold orebodies in the drill cores (Fig. 3). The alteration and mineralization of the granite porphyry in the contact zone also indicate that the granite porphyry is basically contemporaneous with mineralization. The zircon U-Pb age of 242 ± 2 Ma for the granitic porphyry can indirectly constrain the mineralization time of Taijiying. Therefore, the Taijiying gold deposit likely formed in the Middle Triassic.

Episodes of metallogenic events occurred on the northern margin of the NCC (Zhang et al. 2018) at 220–250 Ma and 120–140 Ma (Fig. 11a) with magmatism at 220–240 Ma, 150–170 Ma, and 115–130 Ma (Appendix B, C). Despite of some similarities (Appendix D), the Triassic and Cretaceous gold deposits are distinct in some aspects: (1) subordinate sulfide contents of the gold ores: the Triassic gold deposits show lower contents of the subordinate sulfides than the Cretaceous deposits (Hou 2011; Song et al. 2016); (2) CO_2 contents in the FIs: the gas phase in the early FIs is mainly H_2O + CO_2, whereas the later FIs show only H_2O contents in the gas phase (e.g., Jinchangyu, Song et al. 2016; Jinchanggouliang, Hou 2011); and (3) temperatures and salinities: the mineralization temperatures for the Triassic gold deposits are slightly lower than those for the Cretaceous deposits. In contrast, the salinities exhibit the opposite relationship (e.g., Xiaotazigou, Li et al. 2010). Preliminary analysis suggests that the Taijiying deposit has similar features with the Triassic deposits. Accordingly, the geological features, combined with new dating results, confirm the timing of the mineralization of the Taijiying gold deposit to the Middle Triassic.

5.2. Origin and evolution of ore-forming fluids

At the main ore-forming stages II and III, $\delta^{18}O_W$ values vary from 3.5‰ to 4.8‰ and δD values range from −110‰ to −87‰, which are all lower than those for metamorphic water ($\delta^{18}O_W$ of 5-25‰; δD of −70 to −20‰; Taylor, 1974) and magmatic fluids ($\delta^{18}O_W$ of 5.5-10‰; δD of −80 to −40‰; Sheppard, 1986). In the δD vs. $\delta^{18}Ow$ diagram (Fig. 10b), these values plot below the metamorphic and magmatic fields, but are closer to the magmatic field, as well as the contemporaneous gold deposits such as the Xiaotazigou (Li et al. 2010) and Zhuanshanzi gold deposits in the Chifeng-Chaoyang district (Hou 2011; Sun et al. 2015; Song et al. 2016; Liu et al. 2019a). Particularly, the Xiaotazigou gold deposit was a Triassic magmatic hydrothermal gold deposit with δD values (-82.61‰ – −91.79‰) and $\delta^{18}O_W$ values (5.55‰–7.56‰) (Zhang, 2007). They plot in the area close to the magmatic fluid field (Fig. 10b). In addition, the Triassic Zhuanshanzi gold deposit was identified as typical intrusion-related gold deposits which have average δD value −86.13‰ and $\delta^{18}O_W$ 2.17‰ in the quartz-pyrite stage closing to the magmatic ranges (Fig. 10b). In the quartz-sulfides stage, the δD values dropped to the range of −112.4‰ to −108‰ which are more deficit than magmatic fluids. In the last quartz-calcite stage, the ores had δD values −124.4‰ – −120.1‰ and $\delta^{18}O_W$ values 2.89‰ – −8.09‰.

Table 5
Lead isotopic compositions and its related parameters of sulfide from the Taijiying gold deposit.

Sample	Mineralization stages	Mineral	$\delta^{34}S_{V\text{-}CDT}$/‰	$^{206}Pb/^{204}Pb$	$^{207}Pb/^{204}Pb$	$^{208}Pb/^{204}Pb$	μ	ω	Th/U	Δα	Δβ	Δγ
TJY-G06	Stage II	pyrite	1.8	15.13	15.07	35.79	9.19	41.53	4.37	37.23	4.53	44.45
TJY-G07	Stage II	pyrite	1.9	15.62	15.11	35.87	9.03	37.76	4.05	34.35	−0.11	30.43
TJY-G08	Stage II	pyrite	1.8	15.73	15.12	36.46	9.01	40.34	4.33	34.16	−0.71	43.74
TJY-G09	Stage II	pyrite	2.0	15.80	15.05	36.51	8.82	39.18	4.30	26.81	−6.94	39.16
TJY-G10	Stage II	pyrite	1.8	15.09	15.15	36.73	9.44	49.43	5.07	45.90	12.39	77.06
TJY-G01	Stage III	pyrite	2.1	15.67	15.10	37.97	9.00	49.55	5.33	33.40	−1.08	88.66
TJY-G02	Stage III	pyrite	1.9	15.66	15.11	36.20	9.02	39.39	4.23	34.09	−0.48	38.60
TJY-G03	Stage III	pyrite	1.7	15.72	15.15	36.39	9.09	40.45	4.31	37.54	2.11	43.83
TJY-G04	Stage III	pyrite	1.8	15.10	15.00	35.87	9.03	41.51	4.45	30.73	−0.90	44.85
TJY-G05	Stage III	pyrite	1.9	15.90	15.13	35.76	8.98	35.15	3.79	34.15	−1.39	18.52

This trend indicates that the ore-forming fluids were from a mixing of magmatic fluids with meteoric water (Wang et al., 2016). Sulfur isotopes also support this viewpoint (Wang et al., 2016). The Taijiying gold deposit is within 5 km of the large Late Triassic intrusive bodies in the field (Fig. 2a). Moreover, the close genetic relationship between the Triassic granitic porphyry and gold ore bodies indicates that the magmatic water could have been a primary fluid source. Inputs of metamorphic water cannot be excluded since the magmatic water had gone through the Archean metamorphic rocks into the faults (Pirajno 2007).

The temperatures and salinities of the Taijiying ore-forming fluids show a gradual degradation from the stage I to the stage IV (Fig. 10a). The stage I ore-forming fluids, represented by clouded-white quartz ± pyrite veins, belong to the H_2O-NaCl-CO_2 system with moderate-high temperatures (285–352 ℃) and moderate salinities (6.98–9.10 wt% NaCl eqv). In the stage II, the ore-forming fluids are under conditions of slightly lower temperatures (220–337 ℃) and salinities (2.04–7.29 wt% NaCl eqv) and are gold-rich, as represented by the gray quartz + pyrite veins. The stage III exhibits lower temperatures (228–329 ℃) and slightly higher salinities (4.15–9.80 wt% NaCl eqv), which are represented by quartz + polymetallic sulfide veins. The stage IV of the ore-forming fluids, indicated by calcite ± quartz veins, shows a H_2O-NaCl system with low temperatures (124–223 ℃) and low salinities (2.22–5.79 wt% NaCl eqv). The ore-forming fluids of the stages II and III are characterized by moderate-high temperatures and magmatic hydrothermal fluids with fluctuating salinities. Based on the relationship between salinities and total homogenization temperatures of fluid inclusions (Fig. 10a), salinities of inclusions generally decrease with decreasing homogenization temperatures, indicating a fluid evolution involving cooling and mixing. The evolution trend of salinity and temperature is not completely linear, and some inclusions of stage II show lower salinities at higher temperatures from 210 ℃ to 330 ℃. These situations indicate at least two end-member fluids mixing: (1) magmatic fluid with high temperature and high salinity, and (2) a lower temperature and low salinity H2O-rich fluid (Yao et al., 1999). Mixing of magmatic and meteoric fluids is also suggested by hydrogen and oxygen isotope compositions of ore (Fig. 10b). In general, most of gold deposits including Taijiying in Chifeng-Chaoyang district have moderate-high temperatures and low salinities fluids which are distinct from those of typical porphyry or skarn deposits with high temperatures (400–600 ℃) and high salinities (30–60 wt% NaCl eqv)(Kerrich et al., 2000). Previous works suggest that these fluid types may be the end-members involved (Yao et al., 1999). The low temperatures and salinities document the influx of the meteoric water and the transition of the magmatic hydrothermal system, as also evidenced by the low-temperature calcite veining in the last stage.

Different FI types coexisting in the quartz-sulfide veins at the stages II and III (Fig. 9b-f) indicates fluid phase separation or immiscibility in the Taijiying deposit, which is also supported by the microthermometric data: (1) the coexistence of the type 1 and type 3 FIs shows a similar temperature range with opposite homogenization modes (vapor phase and liquid phase, respectively); (2) the variations in the salinity of the type 2 FIs reflect phase separation or immiscibility of fluids (Lu 2011). The initial hydrothermal fluids at the stage I were likely carbonic fluids according to the existence of the vapor-rich FIs in the quartz veins. The existence of the type 1 and type 2 FIs in stages II and III quartz indicates that the two stages of the ore-forming fluids were CO_2-rich. However, the stage IV quartz is dominated by the type 3 FIs, indicating that the final stage fluids were CO_2-poor. Hence, the H_2O-NaCl-CO_2 ore-forming fluids could have evolved from CO_2-rich to CO_2-poor through CO_2 degassing, fluid immiscibility, and meteoric water influx. Carbonic acids (H_2CO_3, HCO^-, and CO^-), which are the aqueous species of CO_2 according to pH, act as pH buffers (Phillips and Evans 2004) by maintaining fluids in the optimal range of gold solubility close to neutral pH values. The decreasing content of CO_2 facilitates the fluids to be more acidic, leading to the breakdown of the gold bisulfide complexes and precipitation (Gaboury 2019).

In summary, the ore-forming fluids of the Taijiying gold deposit belong to a H_2O-NaCl-CO_2 magmatic water system under moderate-high temperatures and moderate-low salinities.

5.3. Source of ore-forming materials

The average $\delta^{34}S$ value of sulfides can represent that of the total sulfur when the mineral association is simple (Ohmoto and Rye 1979). The mapping of pyrite demonstrates that gold was sourced from primary pyrite (Large et al. 2007, 2012). Pyrite is the dominant sulfide, making up more than 85% of the sulfide in the Taijiying gold deposit so that sulfur isotopic composition could be used to constrain the source of sulfur in ore-forming fluids. Ten sulfur isotope analyses for the pyrites from the main stages II and III in the Taijiying gold deposit yield a narrow range of $\delta^{34}S$ values from + 1.7 to + 2.1 ‰ (average = +1.9 ‰) (Table 5), which indicates that the sulfur was likely originated from a uniform source reservoir. This range of $\delta^{34}S$ values in the sulfide minerals has been interpreted to be originated from a common sulfur reservoir such as mantle-derived magmatic rocks, average crustal sulfur, or metamorphosed sedimentary sulfur (Fig. 11b; Appendix E; Ridley and Diamond 2000; Chang et al. 2008). Such a narrow range of sulfur isotopic values close to 0‰ implies a magmatic source in the Taijiying hydrothermal deposits (Ohmoto and Rye 1979). The amphibolite-facies to granulite-facies metamorphic supracrustal sequences in the Archean Jianping Group (Liu et al. 2011) might have been the sources of metals under metamorphic reactions at the greenschist-amphibolite boundary (Zhong et al. 2015; Yakymchuk 2017; Kresse et al. 2018; Gaboury 2019), but the metamorphic reaction predated the gold mineralization by ca. 2.0 Ga. Therefore, significant contamination or assimilation of metamorphic rock sulfur is lacking, implying that the S sources of the sulfides are of a magmatic origin in the Taijiying gold deposit.

Low concentrations of U and Th, and unradiogenic Pb isotopes enable the Pb isotope data of the sulfides as a useful geochemical tool to constrain the source of Pb (Bozkaya, 2011; Goldfarb et al., 2004). The Pb isotope compositions of the pyrites from the quartz-sulfide veins in the Taijiying gold deposit were compiled, having $^{206}Pb/^{204}Pb$ values of 15.088–15.895, $^{207}Pb/^{204}Pb$ values of 15.001–15.147, and $^{208}Pb/^{204}Pb$ values of 35.758–37.970 (Table 5). The pyrites are characterized by

Table 6
Re-Os isotopic compositions of pyrite from the Taijiying gold deposit.

Sample No.	Weight (g)	Re/ppb	2σ	Os_{total}/ppb	Os_{common}/ppb	2σ	^{187}Re/ppb	2σ	^{187}Os/ppb	2σ	$^{187}Re/^{188}Os$	2σ	$^{187}Os/^{188}Os$	2σ	Age Ma	2σ
TJY-NL02	0.65026	3.88	0.03	0.05	0.02560	0.00025	2.440	0.018	0.02063	0.00017	732.6	8.6	6.196	0.022	505.4	5.4
TJY-NL03	0.65028	15.14	0.11	0.07	0.01168	0.00009	9.513	0.070	0.05638	0.00043	6259	64	37.082	0.069	354.7	3.6
TJY-NL04	0.65002	10.96	0.08	0.06	0.01804	0.00014	6.890	0.051	0.04554	0.00034	2936	30	19.387	0.034	395.4	4.0
TJY-NL06	0.65000	0.76	0.01	0.03	0.02275	0.00019	0.475	0.004	0.00965	0.00008	160.6	1.7	3.251	0.013	449.4	4.9
TJY-NL01	0.30000	1.44	0.01	0.01	0.00371	0.00003	0.906	0.007	0.00600	0.00005	1878	19	12.441	0.035	396.0	4.0

homogeneous radiogenic Pb isotopes, poor in U-radiogenic Pb, and rich in Th-radiogenic Pb (Table 5, Th/U = 3.79–5.33). The μ values (8.82–9.19) are in the range of the upper crust (9.58) and the mantle (8–9), implying that Pb was derived from the lower crust (Zartman and Doe 1981). The relatively unradiogenic Pb isotopes are highly distinct from those of NE China, but similar to those of the NCC (Zartman and Doe 1981; Zhang 1995; Zhang et al. 2013; Fig. 11c, d; Appendix F), implying that the source of metals is likely to be NCC. The Pb isotopic ratios of the Mesozoic and Cenozoic basalts from the Chifeng-Chaoyang district (Zhou et al. 2001; Li et al. 2002; Wu et al. 2003; Zhang et al. 2005b) reflect the mantle signatures of the NCC (Zartman and Haines 1988). In contrast, the values of the Taijiying gold deposit are similar to those of the lower crust and the Jianping Group (Wang and Tang 1994; Sun 2013). The Pb-isotope compositions of the Jinchanggouliang Triassic diorite are distinct in comparison with those of the Taijiying gold deposit, suggesting that the ore-forming metals of the Taijiying gold deposit were not directly related to the contemporaneous mantle-derived magmatism. The origin of ore formation in the Triassic Jinchangyu gold deposit has been reported to be related to lower crust, which has Pb-isotope compositions similar to those of the Taijiying gold deposit (Fig. 11c, d; Song et al. 2016). Xiong et al. (2020) compiled the Pb isotopes of representative gold deposits from the eastern Yanshan belt and propose that ore-forming metals of the Mesozoic lode gold deposits originated from metal-fertilized lower crust. In addition, a weighted average value of initial $^{187}Os/^{188}Os$ ratio yields 2.3 ± 1.0 for the studied pyrites (MSWD = 61, Table 6), which can be used to determine the origin of the metals (Song et al. 2016). The initial $^{187}Os/^{188}Os$ value is obviously distinct from the ratio of the primary mantle (0.105–0.152, Walker et al. 1994; Shirey and Walker 1998), but close to the range of the crust (0.8–1.3) (Esser and Turekian 1993; Marcantonio et al. 1993), indicating that the ore-forming metals were mainly derived from crust-derived magmatism. Therefore, the signatures of the S-Pb-Os isotope compositions indicate that the metals in the Taijiying gold deposit were mainly sourced from the magma derived from the partial melting of the lower crust.

5.4. Genesis of the Taijiying gold deposit

The genesis of the Taijiying deposit remains ambiguous, with different models advocating a metamorphic or magmatic hydrothermal origin. To clarify the genetic type of the Taijiying gold deposit, the geological signatures, fluid inclusions, and isotopes of the Taijiying gold deposit and other gold deposits in the Chifeng-Chaoyang district are listed in Appendix D. Major features include: (1) the gold ore bodies formed in the Early Mesozoic subduction setting (Chen et al. 2006; Zeng et al. 2009) and are controlled by a series of subordinate fracture systems of the deep faults, which is similar to the other gold deposits in the district (e.g., the Xiaotazigou deposit, Li et al., 2010; the Jinchanggouliang deposit, Hou et al. 2011); (2) the wall rock alterations are mainly silicification, sericitization, pyritization, and chloritization, with minor carbonatization, which are consistent with those of the mesothermal magmatic hydrothermal gold deposits (e.g. Jinchanggouliang-Erdaogou, Miao et al., 2003); (3) the H-O isotopes are close to the magmatic field; (4) the sulfide $\delta^{34}S$ values range from 1.7 to 2.1 ‰ (average = +1.9 ‰), indicative of a magmatic source; (5) the Pb and Os isotopic compositions of the Au-bearing pyrites suggest that the metals were derived from the lower crust; (6) the H_2O-NaCl-CO_2 ore-forming fluids are characterized by moderate-high temperatures (124–352 ℃) and a large variation of salinities (2.22–9.80 wt% NaCl eqv.). Therefore, we infer that the deposit is probably of a magmatic hydrothermal origin based on the geological characteristics and spatial–temporal relationship with the intrusions.

The relationship between the intrusions and the gold mineralization needs to be considered when evaluating the ore-forming fluids. As mentioned above, the Triassic magmatism took place in the ore field as dikes and in the surrounding area as large batholiths. Precise U-Pb

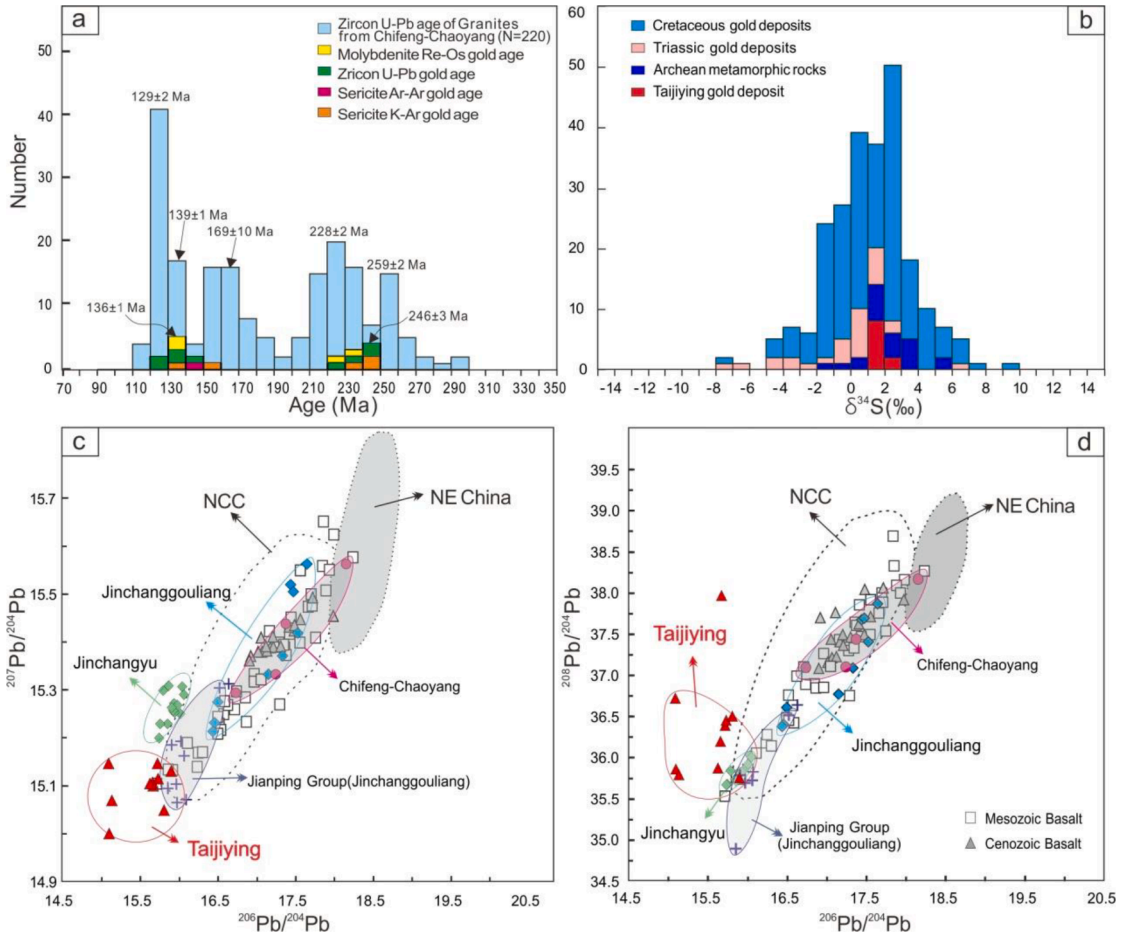

Fig. 11. a, Histograms of ages of Late-Paleozoic and Mesozoic granitoids and gold deposits from Chifeng-Chaoyang district. b, Sulphur isotopic compositions of major gold deposits and metamorphic rocks from Chifeng-Chaoyang district. c–d, Lead isotope plots for the Taijiying Au deposit. Lead isotopic data of gold deposits in the Chifeng-Chaoyang area from Wang et al.(2016); Jinchanggouliang lead isotope data are from Wang et al.(1994) and Sun et al.(2013); Those of the Mesozoic basalts from Wang (1994), Zhou et al. (2001), Wu et al.(2003) and Zhang et al.(1998); Cenozoic basalts from Zhang et al.(2005b).

geochronology records an age of ca. 240 Ma for the granitic porphyry dike in Taijiying, possibly constraining the gold mineralization as the Middle Triassic. Furthermore, within 5 km to the north and northwest, the emplacement of the Triassic granite batholith might have inevitably affected or controlled the gold mineralization. The above geological and isotopic evidence indicates that the Taijiying gold deposit is likely a magmatic hydrothermal gold deposit related to the Triassic granitic magamtism.

A possible genetic scenario for the Taijiying gold deposit is illustrated in Fig. 12. Geochronological, petrological, and structural studies show that the convergence between the Siberian Plate and the NCC took place during the late Permian and the Middle Triassic (Chen et al., 2009; Xiao et al., 2009). The Taijiying Au deposit can be attributed to the far field stresses during the continent–continent collision of North China and Siberia along the northern margin of the NCC in the Early Mesozoic. A series of deep and large NNE trending faults superimposed on the EW trending faults and formed a large number of rhomboid fault basins. Meanwhile, the main tectonic direction in this area began to change from EW to NE/NNE. At the intersection of the fault zone, different types of granitic intrusive rocks are scattered. Some of them have close spatial relationship with the gold mineralization zone. Tectonic reactivation of the cratonic margin and gold deposition coupled with magmatism were associated with asthenospheric melting triggered by lithosphere delamination (Fig. 12a). The diorite and granitic batholith and dike intruded into the Archean metamorphic rocks along the pre-existing faults. The Taijiying gold depsoit is believed to be spatially and temporally related to this magmatic event. The magmatic hydrothermal fluids evolving from the granitic magmas provided not only metals and fluids but also external heat to promote the gold-rich fluids upward, leading to the deposition with mixed features of the magmatic and meteoric fluids. Late gold precipitation occurred when the fluids were migrated along the deep-seated faults to the low-pressure zones created by the transition from the plastic to brittle deformation. The change of the physical–chemical conditions resulted in the precipitation of abundant gold along the faults (Fig. 12b).

The Taijiying gold deposit underwent fault-controlled magmatic hydrothermal mineralization, which might represent a distal expression of the Triassic magmatic activity in the Chifeng-Chaoyang district. Regionally, the difference in the sources of the ore-forming fluids and metals between the Triassic gold deposits and the orogenic ones indicates that deposits in the Chifeng-Chaoyang gold district might not be the typical orogenic gold deposits. The magmatic activities instead of the metamorphic fluids play the key role in the gold mineralization. Thus, areas documenting the Triassic batholiths with a developed fault system would be prospective targets for locating gold deposits.

Regionally, the gold mineralization of the Chifeng-Chaoyang gold district is multiple periods from Middle-Late Triassic to Cretaceous (Zhu et al., 2017; Zhang et al., 2018), which might be controlled by the interaction between the NCC and the surrounding terranes or plates. The Early Mesozoic tectonic setting in the northern margin of NCC was always effected by the evolution of CAOB (Goldfarb et al., 2014), and the contemporaneous gold deposits were related to post-collisional/post-

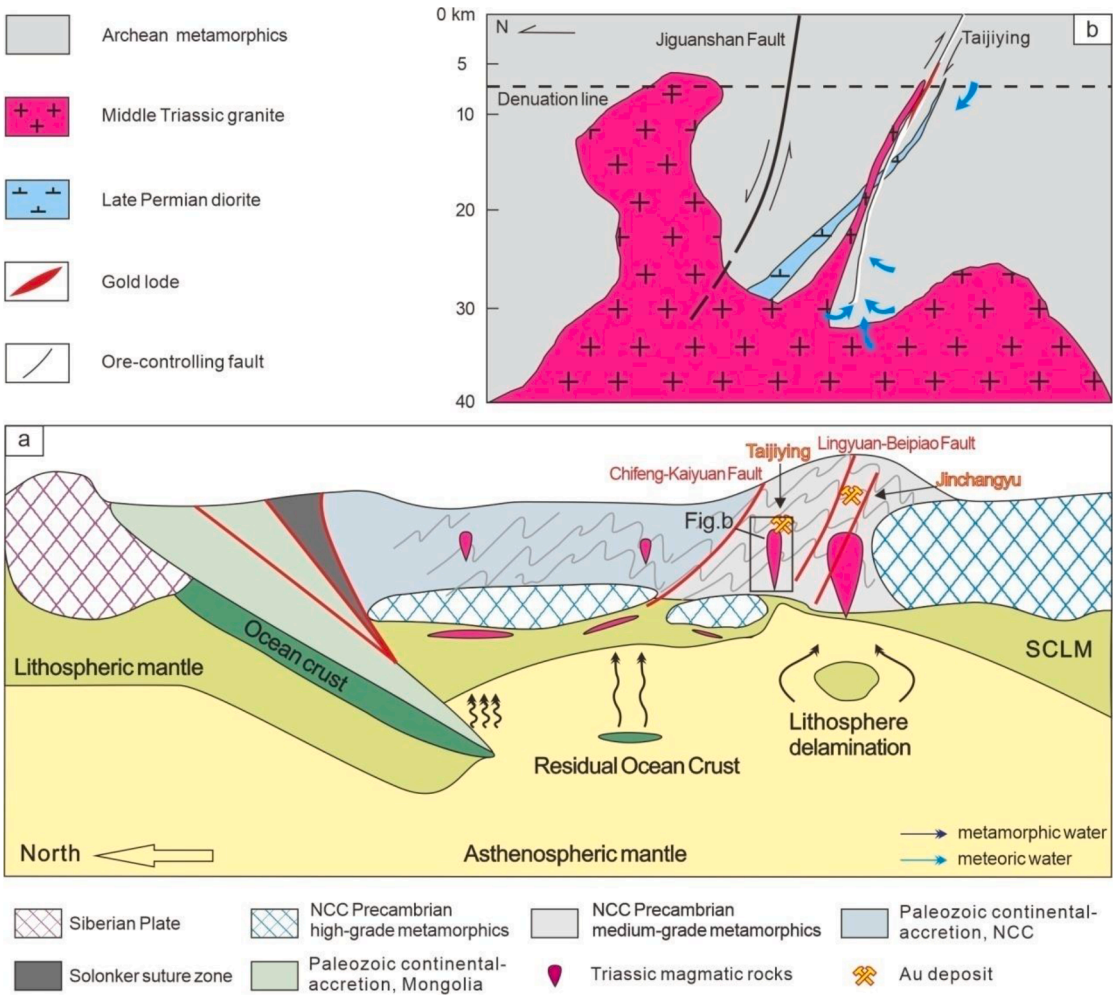

Fig. 12. a, Tectonic-metallogenic model for the Taijiying Au deposit in Triassic (after Song et al. 2016, Li et al., 2020b, Nie et al. 2011, and Xiao et al. 2003). The Taijiying Au deposit can be attributed to the continent–continent collision and extension of northern China and Siberian Plate along the northern margin of the NCC in the Early Mesozoic. b, A possible genetic model for Triassic gold mineralization in the Chifeng-Chaoyang district.

orogenic extension after the final closure of the Paleo-Asian Ocean and amalgamation of the Mongolian arc terranes with the northern margin of NCC (Zhang et al., 2009c). The Triassic tectonic activation in the Chifeng-Chaoyang district is represented by a series of fold structures, thrust faults, ductile shear zones, schistosity zones and magmatism (Nie et al., 2011; Meng et al., 2020). The Early Mesozoic mafic–ultramafic complexes and their Sr-Nd-Hf isotopic compositions indicate the asthenospheric mantle become more significant from Early to Late Triassic, owing to strong upwelling of asthenospheric mantle and post-collisional lithospheric delamination (Zhang et al., 2009c). A series of Triassic acid and alkaline rocks also indicate that obvious lithospheric delamination and asthenosphere upwelling may have occurred during the Late Triassic, which may represent the beginning of lithospheric thinning in the northern margin of the NCC (Yang et al., 2012). The magmatic hydrothermal mineralization, including the Taijiying gold deposit, would be the response to the initial destruction of the NCC in the Early Mesozoic. During the Cretaceous, the geological evolution of the NCC was dominated by the subduction of the Paleo-Pacific Plate, which caused the peak decratonization and led to large-scale magmatism and mineralization of gold deposits. Accordingly, the Triassic and Cretaceous gold deposits in the Chifeng-Chaoyang gold district might reflect the different stages of cratonic destruction of the NCC.

6. Conclusions

(1) The Triassic Taijiying gold deposit is hosted in a series of compressional or extensional faults. The mineralization processes can be divided into four stages: (I) clouded-white quartz ± pyrite, (II) gray quartz + pyrite, (III) quartz + polymetallic sulfides, and (IV) calcite ± quartz, with gold being mainly hosted at the stage II.

(2) The H_2O-NaCl-CO_2 ore-forming fluids of the main stages II and III was characterized by moderate-high temperatures (283-315℃) and low-moderate salinities (< 7 wt% NaCl eqv.), and had a primary magmatic source.

(3) The features of the S-Pb-Os isotopes indicate that the Taijiying ore-forming metals were mainly sourced from the magma derived from the partial melting of the lower crust.

(4) Geological and isotopic evidence suggests that the Taijiying gold deposit is probably a magmatic hydrothermal deposit. The areas recording the Triassic intrusions coupled with a developed fault system may represent prospective targets for locating gold deposits in the Chifeng-Chaoyang gold district.

Declaration of Competing Interest

The authors declare that they have no known competing financial interests or personal relationships that could have appeared to influence

the work reported in this paper.

Acknowledgements

This work was supported by the National Key Research and Development Program of China [Grand Numbers 2018YFC0603702; 2016YFC0600106], and the Geological Survey Program of China [Grand Numbers DD20190685]. Special thanks are due to Doctor Zhang Min for her assistances in fluid inclusion analyses and the stuffs of TIANHE CHEMICALS Ltd. for their logistic and technical support during sampling in the mining areas.

Appendix A. Supplementary data

Supplementary data to this article can be found online at https://doi.org/10.1016/j.oregeorev.2021.104593.

References

Bark, G., Boyce, A.J., Fallick, A.E., Weihed, P., 2020. Fluid and metal sources in the Fäboliden hypozonal orogenic gold deposit, Sweden. Miner. Deposita 1–16.
Belousova, E., Griffin, W., O'Reilly, S.Y., Fisher, N., 2002. Igneous zircon: trace element composition as an indicator of source rock type. Contrib Mineral Petr 143 (5), 602–622.
Brown, P.E., Hagemann, S.G., 1995. MacFlinCor and its application to fluids in Archean lode-gold deposits. Geochim Cosmochim AC 59 (19), 3943–3952.
Brown, P.E., Lamb, W.M., 1989. P-V-T properties of fluids in the system $H_2O \pm CO_2 \pm$ NaCl: New graphical presentations and implications for fluid inclusion studies. Geochim Cosmochim AC 53 (6), 1209–1221.
Chang, Z., Large, R.R., Maslennikov, V., 2008. Sulfur isotopes in sediment-hosted orogenic gold deposits: Evidence for an early timing and a seawater sulfur source. Geology 36 (12), 971. https://doi.org/10.1130/G25001A.110.1130/2008242.
Chen, J.S., Li, W.W., Liao, M., Xing, D.H., Yang, J.L., 2015. U-Pb Isotopic Age of the Vocanic Rocks of the Yixian Formation in Jianping Machang of Western Liaoning and Its Geological Significance. Journal of Jilin University: Earth Science Edition 45, 471–482 (in Chinese with English abstract).
Chen, Y.-J., Pirajno, F., Qi, J.-P., 2008. The Shanggong gold deposit, Eastern Qinling Orogen, China: Isotope geochemistry and implications for ore genesis. J Asian Earth Sci 33 (3-4), 252–266.
Chen, Y.J., Zhai, M.G., Jiang, S.Y., 2009. Significant achievements and open issues in study of orogenesis and metallogenesis surrounding the North China continent. Acta Petrologica Sinica 25 (11), 2695–2726 (in Chinese with English abstract).
Chen YJ, Pirajno F, Qi JP, Li J, Wang HH (2006) Ore geology, fluid geochemistry and genesis of the Shanggong gold deposit, eastern Qinling Orogen, China. Resour Geol 56: 99–116.
Clayton R, Bloomquist A (1973) Friction reducing in flowing hydrocarbon fluids. U.S. Patent No. 3,779,969. Washington, DC: U.S. Patent and Trademark Office.
Deng, J., Yang, L.Q., Li, R., Groves, D.I., Santosh, M., Wang, Z.L., Sai, S.X., Wang, S.R., 2017. Regional structural control on the distribution of world-class gold deposits: An overview from the Giant Jiaodong Gold Province. China. Geological Journal 54 (1), 378–391.
Esser, B.K., Turekian, K.K., 1993. The osmium isotopic composition of the continental crust. Geochim. Cosmochim. Acta 57 (13), 3093–3104.
Fu, L.B., Wei, J.H., Chen, H.Y., Bagas, L., Tan, J., Li, H., Zhang, D.H., Tian, N., 2016. The relationship between gold mineralization, exhumation of metamorphic core complex and magma cooling: Forming of the Anjiayingzi Au deposit, northern North China Craton. Ore Geol. Rev. 73, 222–240.
Fu, L.B., Wei, J.H., Kusky, T.M., Chen, H.Y., Tan, J., Li, Y.J., Shi, W.J., Chen, C., Zhao, S. Q., 2012. The Cretaceous Duimiangou adakite-like intrusion from the Chifeng region, northern North China Craton: Crustal contamination of basaltic magma in an intracontinental extensional environment. Lithos 134–135, 273–288.
Fu, L.B., Wei, J.H., Bagas, L., Franco, P., Zhao, X., Chen, J.J., 2020. Multistage exhumation of the Anjiayingzi gold deposit, northern North China Block: Geodynamic settings and exploration implications. Ore Geol. Rev. 116, 103220.
Gaboury, D., 2019. Parameters for the formation of orogenic gold deposits. Appl. Earth Sci. 128 (3), 124–133.
Goldfarb, R.J., Snee, L.W., Pickthorn, W.J., 1993. Orogenesis, HighT Thermal Events, and Gold Vein Formation within Metamorphic Rocks of the Alaskan Cordillera. Mineralogical Magazine - MINER MAG 57 (388), 375–394.
Goldfarb, R.J., Baker, T., Dube, B., Groves, D.I., Hart, C.J., Gosselin, P., 2005. Distribution, character and genesis of gold deposits in metamorphic terranes. Economic Geology 100th Anniversary 407–450.
Goldfarb, R.J., Taylor, R.D., Collins, G.S., Goryachev, N.A., Orlandini, O.F., 2014. Phanerozoic continental growth and gold metallogeny of Asia. Gondwana Res. 25 (1), 48–102.
Goldfarb, R.J., Groves, D.I., 2015. Orogenic gold: Common or evolving fluid and metal sources through time. Lithos 233, 2–26.
Goldfarb, R.J., Groves, D.I., Gardoll, S., 2001. Orogenic gold and geologic time: a global synthesis. Ore Geol. Rev. 18 (1-2), 1–75.
Goldfarb, R.J., Newberry, R.J., Pickthorn, W.J., Gent, C.A., 1991. Oxygen, hydrogen, and sulfur isotope studies in the Juneau gold belt, southeastern Alaska; constraints on the origin of hydrothermal fluids. Econ. Geol. 86 (1), 66–80.
Goldfarb, R.J., Qiu, K., Deng, J., Chen, Y.J., Yang, L.Q., 2020. Orogenic gold deposits of China. SEG Spec. Pub 22 (1).
Groves, D.I., Goldfarb, R.J., Gebre-Mariam, M., Hagemann, S.G., Robert, F., 1998. Orogenic gold deposits: A proposed classification in the context of their crustal distribution and relationship to other gold deposit types. Ore Geol. Rev. 13 (1-5), 7–27.
Groves, D.I., Santosh, M., Deng, J., Wang, Q., Yang, L., Zhang, L., 2020. A holistic model for the origin of orogenic gold deposits and its implications for exploration. Miner. Deposita 55 (2), 275–292.
Hammond, N.Q., Robb, L., Foya, S., Ishiyama, D., 2011. Mineralogical, fluid inclusion and stable isotope characteristics of Birimian orogenic gold mineralization at the Morila Mine, Mali, West Africa. Ore Geology Reviews - ORE GEOL REV 39 (4), 218–229.
Hart, C.J., Goldfarb, R.J., Qiu, Y., Snee, L., Miller, L.D., Miller, M.L., 2002. Gold deposits of the northern margin of the North China Craton: multiple late Paleozoic-Mesozoic mineralizing events. Miner. Deposita 37 (3), 326–351.
Hoskin, P.W.O., Schaltegger, U., 2003. The Composition of Zircon and Igneous and Metamorphic Petrogenesis. Rev. Mineral. Geochem. 53 (1), 27–62.
Hou, W.R., 2011. Contrast Study on the Hadamengou Gold Deposit and Jinchanggouliang Gold Deposit, Inner Mongolia. Chinese Academy of Geological Sciences, pp 224 (in Chinese with English abstract).
Kerrich, R., 1989. Archean gold: Relation to granulite formation or felsic intrusions? Geology 17 (11), 1011–1015.
Kerrich, R., Goldfarb, R., Groves, D., Garwin, S., Jia, Y., 2000. The characteristics, origins, and geodynamic settings of supergiant gold metallogenic provinces. Sci. China, Ser. D Earth Sci. 43 (S1), 1–68.
Kresse, C., Lobato, L.M., Hagemann, S.G., Silva, F.E., RC,, 2018. Sulfur isotope and metal variations in sulfides in the BIF-hosted orogenic Cuiabá gold deposit, Brazil: Implications for the hydrothermal fluid evolution. Ore Geol. Rev. 98, 1–27.
Kröner, A., Cui, W.Y., Wang, S.Q., Wang, C.Q., Nemchin, A.A., 1998. Single zircon ages from high-grade rocks of the Jianping Complex, Liaoning Province, NE China. J. Asian Earth Sci. 16 (5-6), 519–532.
Large, R.R., Maslennikov, V.V., Robert, F., Danyushevsky, L.V., Chang, Z., 2007. Multistage Sedimentary and Metamorphic Origin of Pyrite and Gold in the Giant Sukhoi Log Deposit, Lena Gold Province. Russia. Economic Geology 102 (7), 1233–1267.
LBGMR, 1989. Regional geology of Liaoning province. Geological Publishing House, Beijing, pp. 317–520.
Li, B.L., Xu, Q.L., Zhang, H., Chang, G.L., 2010. A Study of ore-forming fluid features and metallogenesis of 1# vein from Xiaotazigou gold deposit, Chaoyang city, Liaoning Province. Earth Sci. Front. 17, 295–305 (in Chinese with English abstract).
Li, R., Chen, H., Large, R.R., Zhao, L., Liu, Y., Jiao, J., Xia, X.-P., Yang, Q., 2020a. Ore-forming fluid source of the orogenic gold deposit: Implications from a combined pyrite texture and geochemistry study. Chem. Geol. 552, 119781. https://doi.org/10.1016/j.chemgeo.2020.119781.
Li, R., Yang, J.-H., Wang, H., Zhu, Y.-S., Sun, J.-F., Xu, L., 2020b. Triassic lithospheric modification of the northern North China Craton: Evidences from the composite Kalaqin Batholith and ultramafic-mafic Heilihe Intrusive Complex in Inner Mongolia. Lithos 362-363, 105501. https://doi.org/10.1016/j.lithos.2020.105501.
Li, W.P., Li, X.H., Lu, F.X., Zhou, Y.Q., Zhang, D.G., 2002. Geological characteristics and its setting for volcanic rocks fo early Cretaceous Yixian Formation in western Liaoning province, eastern China. Acta Petrologica Sinica 18 (2), 193–204 (in Chinese with English abstract).
Liu, L., Gu, X.-xiang., Zhang, Y.-mei., Ouyang, X., Wang, L.-zhi., Gao, L.-ye., 2019a. Genesis of the Jinchanggouliang gold deposit, Chifeng, China: Constraints from fluid inclusions and isotopic geochemistry. Ore Geol. Rev. 115, 103180. https://doi.org/10.1016/j.oregeorev.2019.103180.
Liu, J., Liu, F.-X., Li, S.-H., Lai, C.-K., 2019b. Formation of the Baiyun gold deposit, Liaodong gold province, NE China: Constraints from zircon U-Pb age, fluid inclusion, and C-H-O-Pb-He isotopes. Ore Geol. Rev. 104, 686–706.
Liu, S., Santosh, M., Wang, W., Bai, X., Yang, P., 2011. Zircon U-Pb chronology of the Jianping Complex: Implications for the Precambrian crustal evolution history of the northern margin of North China Craton. Gondwana Res. 20 (1), 48–63.
Lu, H.Z., 2011. Fluids immiscibility and fluid inclusions. Acta Petrologica Sinica 027 (005), 1253–1261.
Mao, J.W., Li, Y.Q., Goldfarb, R., He, Y., Zaw, K., 2003a. Fluid Inclusion and Noble Gas Studies of the Dongping Gold Deposit, Hebei Province, China: A Mantle Connection for Mineralization? Econ. Geol. 98 (3), 517–534.
Mao, J., Wang, Y., Zhang, Z., Yu, J., Niu, B., 2003b. Geodynamic settings of Mesozoic large-scale mineralization in North China and adjacent areas. Science in China Ser D 46 (8), 838–851.
Marcantonio, F., Zindler, A., Reisberg, L., Mathez, E.A., 1993. Re-Os isotopic systematics in chromitites from the Stillwater Complex, Montana, USA. Geochemica et Cosmochimica Acta 57 (16), 4029–4037.
Mccuaig, T.C., Kerrich, R., 1998. P-T-t deformation fluid characteristics of lode gold deposits: evidence from alteration systematics. Ore Geol. Rev. 12 (6), 381–453.
McFarlane, C.R.M., Mavrogenes, J., Lentz, D., King, K., Allibone, A., Holcombe, R., 2011. Geology and Intrusion-Related Affinity of the Morila Gold Mine, Southeast Mali. Econ. Geol. 106 (5), 727–750.
Meng, Q.-R., Wu, G.-L., Fan, L.-G., Wei, H.-H., Wang, E., 2020. Late Triassic uplift, magmatism and extension of the northern North China block: Mantle signatures in the surface. Earth Planet. Sci. Lett. 547, 116451. https://doi.org/10.1016/j.epsl.2020.116451.

Miao, L.C., et al., 2003. Zircon SHRIMP U-Pb geochronology of the granitoid intrusions from Jinchanggouliang-Erdaogou gold orefield and its significance. Acta Petrologica Sinica(01), 71–80 (in Chinese with English abstract).
Miller, L.D. et al., 1998. North China gold - A product of multiple orogens. Soc Econ Geol Newslett, 33: 1-12.
Nesbitt, B., 1993. Gold Metallogeny and Exploration. Springer, Boston, MA, pp. 104–132.
Nie, F.J., Zhang, K., Liu, Y.F., Jiang, S.H., Liu, Y., 2011. Indosinian Magamtic Activity and Molybdenum, Gold Mineralization along the Northern Margin of North China Craton and Adjacent Area. Journal of Jilin University (Earth Science Edition) 41 (6), 1651–1666 (in Chinese with English Abstract).
Ohmoto, H., Rye, R.O., 1979. Isotopes of sulfur and carbon. Geochemistry of Hydrothermal Ore Deposits 509–567.
Phillips, G.N., Evans, K.A., 2004. Role of CO_2 in the formation of gold deposits. Nature 429 (6994), 860–863.
Phillips, G.N., Powell, R., 2010. Formation of gold deposits: a metamorphic devolatilization model. J. Metamorph. Geol. 28 (6), 689–718.
Piao, S., Wang, L., Li, Q., Yu, Z., Zhang, B., 2007. Study of fluid inclusions in the Xiaotazigou gold deposit. Liaoning. Mineral Resources and Geology 21 (02), 113–117 (in Chinese with English abstract).
Pirajno, F., 2007. Diagnostic fluid inclusions of different types hydrothermal gold deposits. International academic conference on the study of geological fluids and fluid inclusions (C).
Pitcairn, I.K., Craw, D., Teagle, D.A.H., 2015. Metabasalts as sources of metals in orogenic gold deposits. Miner. Deposita 50 (3), 373–390.
POWELL, R., WILL, T.M., PHILLIPS, G.N., 1991. Metamorphism in Archaean greenstone belts: Calculated fluid compositions and implications for gold mineralization. J. Metamorph. Geol. 9 (2), 141–150.
Qiu, K.-F., Yu, H.-C., Deng, J., McIntire, D., Gou, Z.-Y., Geng, J.-Z., Chang, Z.-S., Zhu, R., Li, K.-N., Goldfarb, R., 2020. The giant Zaozigou Au-Sb deposit in West Qinling, China: magmatic- or metamorphic-hydrothermal origin? Miner. Deposita 55 (2), 345–362.
Qu, Y., Yan, Q., He, B., 2015. Three-dimensional Geological 3D Modeling and Reserve Estimate of Taijiying Au Deposit. Geology of Chemical Minerals 37 (01), 28–34 (in Chinese with English abstract).
Ridley JR, Diamond LW (2000) Fluid chemistry of lode-gold deposits, and implications for genetic models, pp 141–162.
Robert, F., 2001. Syenite associated disseminated gold deposit in the Abitibi greenstone belt, Canada. Miner. Deposita 36, 503–516.
Shao, J.A., Zhang, L.Q., Mu, B.L., 1999. Magmatism in the Mesozoic Extending Orogenic Process of DaHinggan MTS. Earth Science Frontiers (China University of Geosciences, Beijing) 6 (4), 339–346 (in Chinese with English Abstract).
Sheppard, S.M.F., 1986. Characterization and Isotopic Variations in Natural Waters. Rev. Mineral. 16 (3), 165–183.
Shirey, S., Walker, R.J., 1998. The Re-Os Isotope System in Cosmochemstry and High-Temprature Geochemistry. Annu. Rev. Earth Planet. Sci. 26, 423–500.
Sibson, R.H., Robert, F., Poulsen, K.H., 1988. High-angle reverse faults, fluid-pressure cycling, and mesothermal gold-quartz deposits. Geology 16 (6), 551. https://doi.org/10.1130/0091-7613(1988)016<0551:HARFFP>2.3.CO;2.
Song, Y., Jiang, S.-H., Bagas, L., Li, C., Hu, J.-Z., Zhang, Q., Zhou, W., Ding, H.-Y., 2016. The geology and geochemistry of Jinchangyu gold deposit, North China Craton: Implications for metallogenesis and geodynamic setting. Ore Geol. Rev. 73, 313–329.
Spence-Jones, C.P., Jenkin, G.R.T., Boyce, A.J., Hill, N.J., Sangster, C.J.S., 2018. Tellurium, magmatic fluids and orogenic gold: An early magmatic fluid pulse at Cononish gold deposit, Scotland. Ore Geol. Rev. 102, 894–905.
Sun, Z.J., 2013. Study on gold deposits mineralization in Chifeng-Chaoyang region, northern margin of north China craton. Jilin University, Changchun, pp. 1–194.
Sun, Z.J., Yu, H.N., Sun, G.S., 2015. Study on Characteristics of Ore-forming Fluids in Chifeng-Chaoyang Gold Belt, Northern Margin of North China Platform. Acta Geologica Sinica (English Edition) 88 (s2), 790–791.
Taylor, H.P., 1974. The Application of Oxygen and Hydrogen Isotope Studies to Problems of Hydrothermal Alteration and Ore Deposition. Econ. Geol. 69 (6), 843–883.
Treloar, P., Lawrence, D., Senghor, D., Boyce, A. and Harbidge, P., 2015. The Massawa gold deposit, Eastern Senegal, West Africa: an orogenic gold deposit sourced from magmatically derived fluids? Geological Society, London, Special Publications, 393.
Walker, R.J., Morgan, J.W., Horan, M.F., Czamanske, G.K., Krogstad, E.J., Fedorenko, V. A., Kunilov, V.E., 1994. Re-Os isotopic evidence for an enriched-mantle source for the Noril'sk-type, ore-bearing intrusions. Siberia. Geochimica et Cosmochimica Acta 58 (19), 4179–4197.
Wang, F.X., Sun, A.Q., Pei, R.F., Liu, Y.F., Jiang, S.H., 2016. Geological, Geochemical Characteristics and the Genetic Mechanism of the Zhuanshanzi Gold Deposit in Inner Mongolia. China. Acta Geologica Sinica 90 (08), 1798–1816 (in Chinese with English Abstract).
Wang, S.Q., Tang, K.L., 1994. The Physicochemical Conditions of Ore-Forming Fluids of Anjiayingzi Gold Deposit, Chifeng, Inner Mongolia. Acta Scientiarum Naturalium Universitatis Pekinensis 30 (4), 446–452 (in Chinese with English Abstract).
Wang, W., Liu, S., Bai, X., Yang, P., Li, Q., Zhang, L., 2011. Geochemistry and zircon U-Pb-Hf isotopic systematics of the Neoarchean Yixian-Fuxin greenstone belt, northern margin of the North China Craton: implications for petrogenesis and tectonic setting. Gondwana Res. 20 (1), 64–81.
Wang, X.S., Zheng, Y.D., 2005. $^{40}Ar/^{39}Ar$ age constraints on the ductile deformation of the detachment system of the Louzidian core complex, southern Chifeng. China. Geological Reveiw 51 (5), 574–582 (in Chinese with English Abstract).
Wu, F.Y., Sun, D.Y., 1999. The Mesozoic Magmatism and Lithospheric Thinning Eastern China. Joural of Changchun University of Science and Technology 29 (4), 313–318 (in Chinese with English Abstract).
Wu, G., Li, Z.Q., Li, Z.T., 2003. Geochemical Characteristics and Genesis of the Early Mesozoic Volcanic Rocks in West Liaoning Area. Journal of Mineralogy and Petrology 23 (3), 44–50 (in Chinese with English Abstract).
Xiao, W., Windley, B.F., Hao, J., Zhai, M., 2003. Accretion leading to collision and the Permian Solonker suture, Inner Mongolia, China: Termination of the central Asian orogenic belt. Tectonics 22 (6), n/a–n/a.
Xiao, W.J., Windley, B.F., Yuan, C., Sun, M., Han, C.M., Lin, S.F., Chen, H.L., Yan, Q.R., Liu, D.Y., Qin, K.Z., Li, J.L., Sun, S., 2009. Paleozoic Multiple Subduction-Accretion Processes of the Southern Altaids. Am. J. Sci. 309 (3), 221–270.
Xiong, L., Zhao, X., Wei, J., Jin, X., Fu, L., Lin, Z., 2020. Linking Mesozoic lode gold deposits to metal-fertilized lower continental crust in the North China Craton: Evidence from Pb isotope systematics. Chem. Geol. 533, 119440. https://doi.org/10.1016/j.chemgeo.2019.119440.
Yakymchuk, C., 2017. Applying phase equilibria modelling to metamorphic and geological processes: recent developments and future potential. Geoscience Canada: Journal of the Geological Association of Canada/Geoscience Canada: journal de l'Association Géologique du Canada 44 (1), 27–45.
Yang, J.H., Wu, F.Y., 2009. Triassic magmatism and its relation to decratonization in the eastern North China Craton. Sci. China, Ser. D Earth Sci. 52 (9), 1319–1330.
Yang, J.-H., Wu, F.-Y., Wilde, S.A., 2003. A review of the geodynamic setting of large-scale Late Mesozoic gold mineralization in the North China Craton: an association with lithospheric thinning. Ore Geol. Rev. 23 (3-4), 125–152.
Yang, J.-H., Sun, J.-F., Zhang, M., Wu, F.-Y., Wilde, S.A., 2012. Petrogenesis of silica-saturated and silica-undersaturated syenites in the northern North China Craton related to post-collisional and intraplate extension. Chem. Geol. 328, 149–167.
Yang, L., Yang, L., Yuan, W., Zhang, C., Zhao, K., Yu, H., 2013. Origin and Evolution of Ore Fluid for Orogenic Gold Traced by DO Isotopes: A Case From the Jiapigou Gold Belt. China. Acta Petrologica Sinica 29 (11), 4025–4035.
Yang, L.Q., Deng, J., Guo, L.N., Wang, Z.L., Li, X.Z., Li, J.L., 2016. Origin and evolution of ore fluid, and gold-deposition processes at the giant Taishang gold deposit, Jiaodong Peninsula, eastern China. Ore Geol. Rev. 72 (1), 585–602.
Yao, Y., Morteani, G., Trumbull, R.B., 1999. Fluid inclusion microthermometry and the P-T evolution of gold-bearing hydrothermal fluids in the Niuxinshan gold deposit, eastern Hebei province. NE China. Mineralium Deposita 34 (4), 348–365.
Zartman, R.E., Doe, B.R., 1981. Plumbotectonics-the model. Tectonophysics 759 (1–2), 135–162.
Zartman, R.E., Haines, S.M., 1988. The plumbotectonic model for Pb isotopic systematics among major terrestrial reservoirs—A case for bi-directional transport. Geochim. Cosmochim. Acta 52 (6), 1327–1339.
Zeng, Q.D., Liu, J.M., Zhang, Z.L., Chen, W.J., Zhang, W.Q., 2011. Geology and geochronology of the Xilamulun molybdenum metallogenic belt in eastern Inner Mongolia, China. Int. J. Earth Sci. 100, 1791–1809.
Zeng, Q.D., Liu, J.M., Zhang, Z.L., Qin, F., Chen, W.J., Zhang, R.B., Yu, C.M., Ye, J., 2009. Ore-forming time of the Jiguanshan porphyry molybdenum deposit, northern margin of North China Craton and the Indosinian mineralization. Acta Petrologica Sinica 25 (2), 393–398 (in Chinese with English Abstract).
Zhai, M.G., Yang, J.H., Fan, H.R., Miao, L.C., Li, Y.G., 2002. A Large-Scale Cluster of Gold Deposits and Metallogenesis in the Eastern North China Craton. Int. J. Earth Sci. 44, 458–476.
Zhai MG, and Zhou YY (2015) General precambrian geology in China. Springer, pp. 3-56.
Zhang, B.W., 2007. Geochemical characteristics and genesis of the Xiaotazigou gold deposit, Liaoning, Jilin University, 72 pp. (in Chinese).
Zhang, B.W., Sun, F.Y., Chang, G.L., Chen, J., 2009a. Discussion on genetic type of Dongwujiazi gold deposit of Chaoyang. Liaoning. Global Geology 28 (3), 297–304 (in Chinese with English Abstract).
Zhang, H.F., Li, S.R., Santosh, M., Liu, J.J., DiWu, C.R., Zhang, H., 2013. Magmatism and metallogeny associated with mantle upwelling: Zircon U-Pb and Lu-Hf constraints from the gold-mineralized Jinchang granite, NE China. Ore Geol. Rev. 54, 138–156.
Zhang LG (1995) Block Geology of Eastern Asia Lithosphere Isotope Geochemistry and Dynamics of Upper Mantle, Basement and Granite. Science Press, Beijing: 1–252(in Chinese with English abstract).
Zhang, L.C., Bai, Y., Zhu, M.T., Huang, K., 2018. Regional Differences of Gold Deposits on the North China Craton. Journal of Earth Science and Environment 40 (4), 363–380 (in Chinese with English abstract).
Zhang, L.C., Wu, H.Y., Xiang, P., Zhang, X.J., Chen, Z., Wan, B., 2010. Ore-forming processes and mineralization of complex tectonic system during the Mesozoic: A case from Xilamulun Cu-Mo metallogenic belt. Acta Petrologica Sinica 26 (5), 1351–1362 (in Chinese with English abstract).
Zhang, S.H., Zhao, Y., Davis, G.A., Ye, H., Wu, F., 2014. Temporal and spatial variations of Mesozoic magmatism and deformation in the North China Craton: Implications for lithospheric thinning and decratonization. Earth-Science Review 131, 49–87.
Zhang, S.H., Zhao, Y., Kröner, A., Liu, X.M., Xie, L.W., Chen, F.K., 2009b. Early Permian plutons from the northern North China Block: constraints on continental arc evolution and convergent margin magmatism related to the Central Asian Orogenic Belt. International Journal of Earth Science 98 (6), 1441–1467.
Zhang, S.H., Zhao, Y., Liu, X.C., Liu, D.Y., Chen, F.K., Xie, L.W., Chen, H.H., 2009c. Late Paleozoic to Early Mesozoic mafic–ultramafic complexes from the northern North China Block: Constraints on the composition and evolution of the lithospheric mantle. Lithos 110 (1–4), 229–246.
Zhang, S.H., Zhao, Y., Song, B., Hu, J.M., Liu, S.W., Yang, Y.H., Chen, F.K., Liu, X.M., Liu, J., 2009d. Contrasting Late Carboniferous and Late Permian-Middle Triassic intrusive suites from the northern margin of the North China craton: Geochronology, petrogenesis, and tectonic implications. Geol. Soc. Am. Bull. 121, 181–200.
Zhang SH, Zhao Y. (2016) Magmatic Records of the Late Paleoproterozoic to Neoproterozoic Extensional and Rifting Events in the North China Craton: A

Preliminary Review. Main Tectonic Events and Metallogeny of the North China Craton. Springer Singapore, Singapore, pp. 359-391.
Zhang, W.H., Han, B.F., Du, W., Liu, Z.Q., 2005. Characteristics of mantle source for Jining Cenozoic basalts from southern Inner Mongolia: evidence from element and Sr-Nd-Pb isotopic geochemistry. Acta Petrological Sinica 21 (6), 1569–1582 (in Chinese with English abstract).
Zhong, R., Brugger, J., Tomkins, A.G., Chen, Y., Li, W., 2015. Fate of gold and base metals during metamorphic devolatilization of a pelite. Geochim. Cosmochim. Acta 171, 338–352.
Zhou, J., Wilde, S.A., 2013. The Crustal Accretion History and Tectonic Evolution of the NE China Segment of the Central Asian Orogenic Belt. Gondwana Res. 23 (4), 1365–1377.
Zhou, X.H., Zhang, G.H., Yang, J.H., Chen, W.J., Sun, M., 2001. Sr-Nd-Pb isotope mapping of Late Mesozoic volcanic rocks across northern margin of North China Craton and implications to geodynamic processes. Geochimica 30 (1), 10–23 (in Chinese with English abstract).
Zhu, R.X., et al., 2017. Craton destruction and related resources. Int. J. Earth Sci. 106, 2233–2257.